The completion of this thesis
was supported by the
Randy Seeling Award
given, in his memory, to another
outstanding graduate student
of the Geology Department,
University of Minnesota, Duluth.

STRUCTURAL ANALYSIS OF ARCHEAN METASEDIMENTARY ROCKS, JARDINE, MONTANA

A THESIS
SUBMITTED TO THE FACULTY OF THE GRADUATE SCHOOL
OF THE UNIVERSITY OF MINNESOTA

BY
JOSEPH DAVID JABLINSKI

IN PARTIAL FULFILLMENT OF THE REQUIREMENTS
FOR THE DEGREE OF
MASTER OF SCIENCE

MAY, 1990

ABSTRACT

The structural history of the Precambrian deformational events in the vicinity of Jardine, Montana, has been reconstructed in some detail. Three phases of folding, as evidenced by minor planar and linear structures, have been recognized in the metamorphosed greywacke and mudstone sequences. The folds developed during the first phase of folding (F_1), were isoclinal and recumbent and likely reached nappe-like scale. A pervasive S_1 schistosity, found in all rock types throughout the region, was formed during, and axial planar to, F_1 folding. S_1 schistosity is a continuous type 1 schistosity that is subparallel to bedding (S_0). The folds developed during the second phase of folding (F_2) were close and nearly upright, with gently to moderately plunging fold axes that trend northeast-southwest. An S_2 zonal crenulation cleavage (symmetric or asymmetric) was formed axial planar to F_2 folds. The folds developed during the third phase of folding (F_3) were open and nearly upright, with gently to moderately plunging fold axes that trend northwest-southeast. A weak S_3 zonal crenulation cleavage (symmetric or asymmetric) was formed axial planar to F_3 folds. Metamorphic mineral growth did not occur during the F_2 and F_3 fold events. The S_2 and S_3 crenulation cleavages are defined by the axial planar alignment of microfold hinges or mica-rich domains. S_2 and S_3 axial surfaces are nearly orthogonal to each other and their intersection is nearly normal to S_1 schistosity. Rare, post-F_3 kink bands were observed. The superposition of the three phases of folding resulted in the formation of a dome and basin (Ramsay type 1) fold interference pattern, observed in the S_1 foliation surface. S_0 displays the same dome and basin pattern, but in addition, small domains near the F_1 fold hinges display a combination of Ramsay type 2 and type 3 fold interference patterns. Calculations from electron microprobe analyses of metamorphic mineral assemblages indicate a peak metamorphic pressure and temperature of approximately 2.9 kb and 560° C. This pressure corresponds to a depth of burial of approximately 10 km. Microfabric observations show that peak metamorphic conditions occurred during or shortly after the first phase of folding. Brittle deformation features (e.g. fault zones, shear zones, joints) observed in the region were formed during the Laramide Orogeny (Late Cretaceous to Early Tertiary).

TABLE OF CONTENTS

LIST OF FIGURES

ACKNOWLEDGMENTS

Many people have influenced my life and given me guidance, encouragement, and support during my academic career. Of course, not everyone can be mentioned below, so for those who are not, I thank them now.

I would like to begin by thanking Doug MacDonald for introducing me to, and getting me excited about, the science of geology. His enthusiasm and energy in and out of the classroom has been an inspiration to me throughout my college education.

I wish to thank my thesis advisor, Dr. Timothy B. Holst, for his direction and patience in the development of this thesis and its author. I have benefitted greatly by having had the opportunity to work closely, both in the field and in the classroom, with Tim.

To Dr. James A. Grant, Dr. Christian P. Teyssier, and Dr. James C. Nichol, I thank them for serving as committee members for this thesis.

A special thanks is given to David C. Oliver, chief geologist at Mineral Hill Mine, whose efforts in coordinating between the University of Minnesota and American Copper and Nickel Company made this research project possible. I would also like to thank David C. Oliver, John Cuthill, William Hofer, and Mark Cechovic for their insightful and enlightening discussions with me concerning the geology of the Jardine region and for their time and patience during the times I tagged along with them underground.

I would like to thank American Copper and Nickel Company, Inc., for their financial support during the summers of 1988 and 1989.

Finally, I would like to thank my fellow graduate students, faculty, and staff at the University of Minnesota, Duluth, for their camaraderie and moral support during my two year internment. It was a pleasure to work and play with them all.

INTRODUCTION

Statement of Problem

The Archean metasedimentary rocks of the southwestern Beartooth Mountains (Figure 1) were affected by multiple ductile deformations during Precambrian regional tectonothermal events at 2700-2800 Ma (Montgomery and Lytwyn, 1984). The purpose of this study is to a) report the style and orientation of the structures formed during Precambrian deformational events in the area around Jardine, Montana (Figure 2); b) determine the relative age relationships between deformational events; and c) show, through structural data collected in the field, the fold interference pattern developed by the superposition of multiple fold events.

This research will provide a structural history of the Precambrian ductile deformations in and around the Jardine area and may also be helpful to future investigators in constructing a more complete and comprehensive structural history of the southwestern Beartooth Mountains.

Method of Study

The study area is a fifteen square mile region surrounding the mine town of Jardine, in Park County, southwestern Montana (Figure 2). Exposures of bedrock in this geologically complex region are very limited ($\leq 5\%$ outcrop) and thus make stratigraphic and/or structural correlations across even moderate distances a futile exercise. Detailed geologic surface mapping of outcrops in the area on a 1 in. =

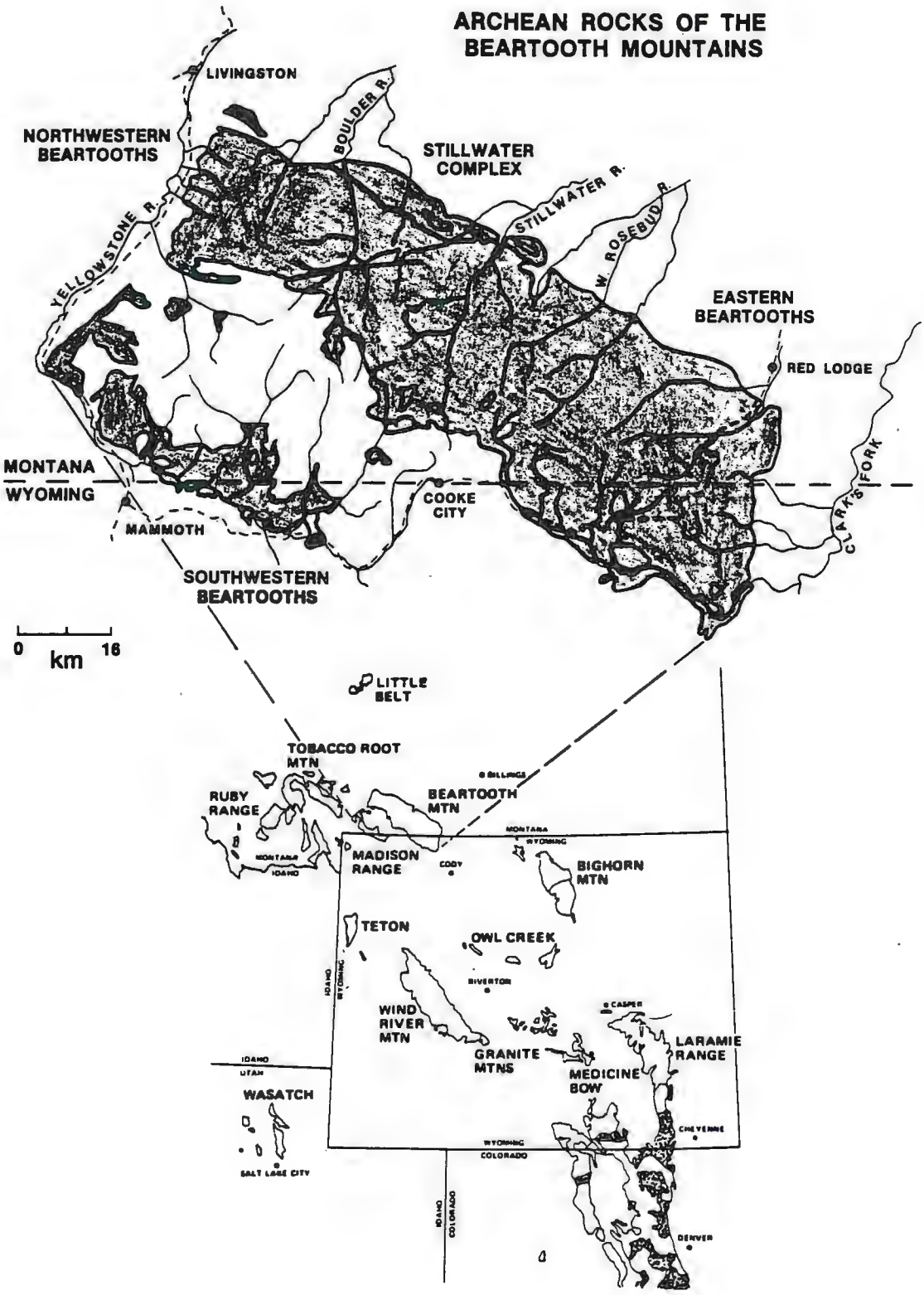

Figure 1. Location of the Beartooth Mountains in the northern Wyoming province (From Mueller et al., 1988).

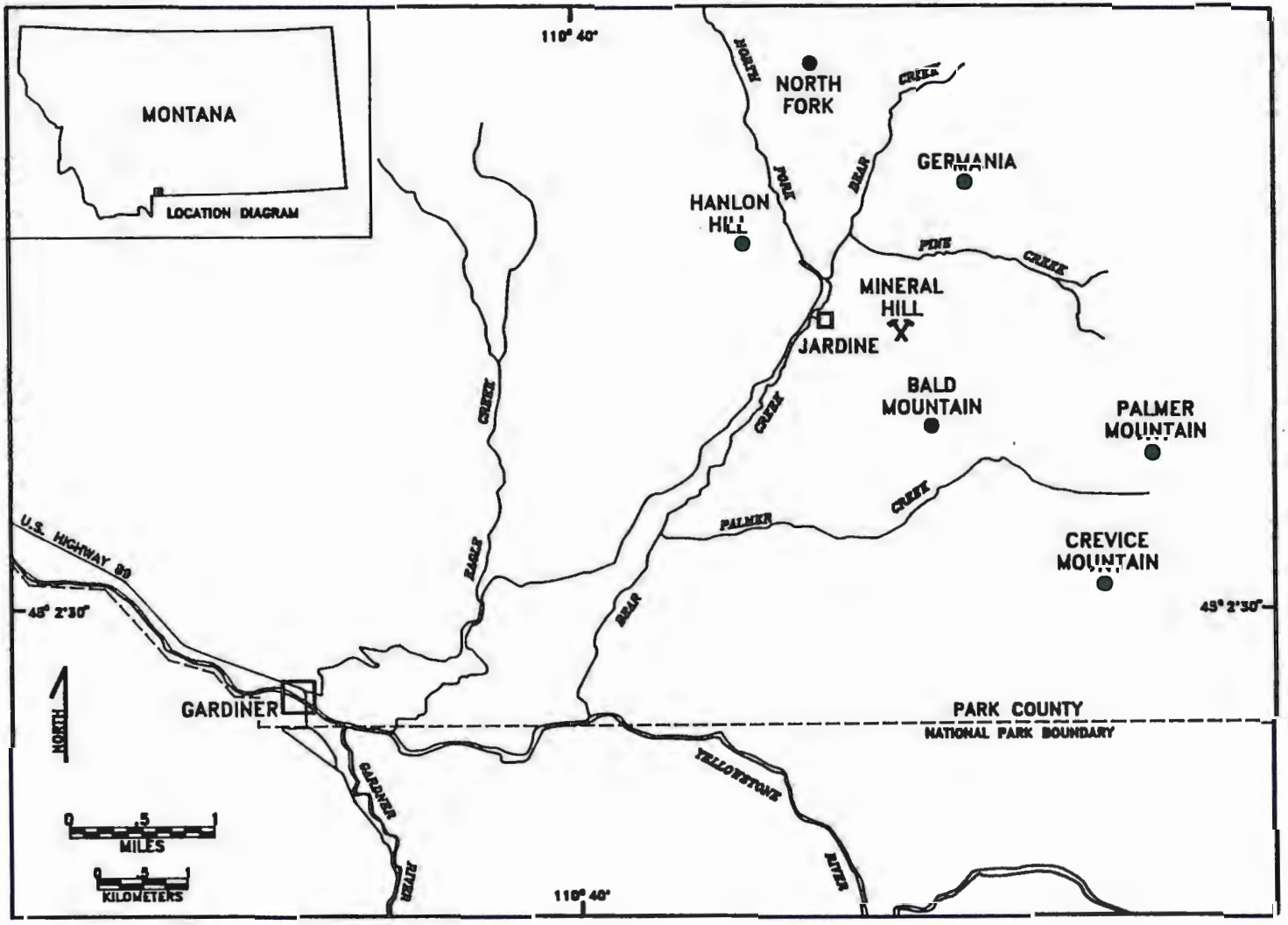

Figure 2. Location of study area.

200 ft. scale was begun by Anaconda Mining Company and Homestake Mining Company, and later completed by American Copper and Nickel Company's geologist, John Ray, in 1985. These maps were used as references for outcrop location and for structural data compilation and correlation during this investigation. Structural data collected during the summers of 1988 and 1989 include measurements of near-bedding-parallel schistosity, axial-planar crenulation cleavages, lineations, and fold axes. Measurements of planar and linear structures, taken from surface outcrops, were plotted on equal-area stereographic nets (Schmidt net) in order to find the orientation of folds produced during Precambrian deformational events. In addition, oriented hand samples from outcrops were collected for thin section microfabric and microprobe analyses.

Previous Work

Previous investigations concentrating exclusively on the Archean metasedimentary rocks of the southwestern Beartooth Mountains are scant at best. Historically, these have been the least studied rocks in the Beartooth Mountains. Following the discovery of Quaternary placer and Precambrian lode gold deposits in this region, a few investigations pertaining to the origin and economic significance of the mineralization in the metasedimentary rocks around the Jardine-Crevice Mountain area have been completed.

George F. Seager (1944) completed an extremely detailed and thorough report on the geology of the Jardine-Crevice Mountain area.

The primary objective of Seager's investigation was to describe evidence for a model in which a hydrothermal alteration event was responsible for the genesis of gold, arsenic, and tungsten mineralization in the metasedimentary rocks around Jardine. In his report, petrographic descriptions of all of the rock types, from the Precambrian basement to the Quaternary volcanic cover, and the structural geology and geologic history of the Jardine-Crevice Mountain area, can be found. Seager's classic work on the area has been an invaluable resource for later investigators working in the region.

A comprehensive discussion of the geology of the Gardiner area was published by Fraser et al. (1969). The emphasis of their work was to investigate the Quaternary reactivation of the Gardiner fault although their report serves as an excellent reference for a description of the stratigraphy of the region and gives a thorough geologic history from the Precambrian to the Holocene.

Hallager's (1980) research also concentrated on the environment of ore deposition/mineralization in the Jardine region. He reports that the ore mineralization may be the result of gold introduced into a seawater environment by nearby ultramafic volcanic activity and that subsequent precipitation of the gold out of the seawater column took place through chemical reactions in a strongly reducing iron-rich environment.

To date, an M.S. thesis by Thurston (1986) is the most recent research completed on the geology of the metasedimentary rocks in the Jardine region. Thurston shows, through geochemical analyses,

that the source for the sediments was mafic to ultramafic. He interprets the high Ni and Cr content in the sediments to indicate a probable source area from an Early Archean greenstone belt. Thurston also reports, using sedimentologic and stratigraphic evidence, that the sediments were deposited on a submarine fan by turbidity currents in an actively subsiding sedimentary basin.

Thurston's geochemical work has contributed to the growing evidence that supports the working hypothesis (Mogk, 1988) that the metasedimentary rocks of the southwestern Beartooth Block were tectonically emplaced into their current position.

Regional Geology

The Beartooth Mountains of southwestern Montana and northwestern Wyoming lie directly north and northeast of Yellowstone National Park and are considered to be part of the northern Wyoming Province in the Middle Rocky Mountains (Figure 1). This forty-by-seventy-mile, west-northwest-trending block of Archean basement was uplifted 10,000-20,000 ft. along steeply-dipping reverse faults during the Laramide Orogeny (Late Cretaceous to Early Tertiary) (Wilson, 1934; Foose et al., 1961).

The Beartooth Mountains can be separated into four regions based largely on lithology and structural style. Those regions are the eastern Beartooth Block, the northwestern Beartooth Block, the Stillwater Block, and the southwestern Beartooth Block (Figure 1).

The eastern Beartooth Block (sometimes referred to as the Beartooth Plateau Block) is composed of Late Archean (2800 Ma)

andesitic amphibolites, granodiorite, and granite with meter- to kilometer-size inclusions of older Archean (probable ages of 3200-3600 Ma) supracrustal rocks (Casella, 1969; Mueller et al., 1985; Wooden et al., 1988). Subduction-related magmatism may be the source for the plutonic rocks that make up the majority of the eastern and central Beartooth Mountains (Mueller et al., 1985; Mogk and Henry, 1988).

The northwestern Beartooth Block (commonly referred to as the North Snowy Block) consists of seven distinct units of metaigneous and metasedimentary rocks (Reid et al., 1975; Mogk et al., 1988). These seven units are distinguished from one another by sharp changes in lithology, metamorphic grade, structural style, and isotopic age (Mogk et al., 1988). It is believed that these units were tectonically juxtaposed by strike-slip or thrust faulting at a continental margin during a Late Archean (2740-2560 Ma) collisional orogeny (Mogk et al., 1988; Mogk, 1988).

The Stillwater Block, which is located along the north-central margin of the Beartooth Mountains, is a sequence of Archean metasedimentary rocks into which a layered mafic and ultramafic intrusive body (the Stillwater Complex), of unknown size and shape, was intruded at about 2700-2720 Ma (Page, 1977; Mogk and Henry, 1988). A contact aureole consisting of fine-layered hornfels, metamorphosed diamictite, blue metaquartzite, and iron formation surrounds the Stillwater Complex (Page, 1977; Page and Zientek, 1985). The Stillwater Block is believed to have been tectonically emplaced alongside the Beartooth Block much like the seven

lithologic units that make up the northwestern Beartooth Block (Page, 1977).

The southwestern Beartooth Block (often referred to as the South Snowy Block) is composed primarily of Archean metasedimentary rocks (2900-3100 Ma; Montgomery and Lytwyn, 1984) into which small granitic stocks and minor mafic dikes and sills have intruded. The protolith of the metasedimentary package has been interpreted as repeating sequences of greywackes and mudstones (Thurston, 1986). Quartz monzonite bodies (i.e. Crevice Mountain Stock, Hellroaring Stock, and Bull Mountain Stock) intruded the metasedimentary rocks approximately 2600-2700 Ma (Brookins, 1968; Montgomery and Lytwyn, 1984). Because the metamorphic grade is unusually low and because the whole-rock geochemistry and structural style are so very different from the surrounding Beartooth Mountains, it is likely that, prior to 2600-2700 Ma, these rocks were tectonically emplaced against the western margin of the Beartooth Block (Mogk, 1988).

The Phanerozoic history of the Beartooth Mountains is much better understood than the Precambrian. From Middle Cambrian time to Late Cretaceous time, approximately 3000 ft. of Paleozoic and 7000 ft. of Mesozoic sedimentary rocks were laid down on the Precambrian crystalline basement of the Beartooth Block (Foose et al., 1961; Fraser et al., 1969). During and shortly after the Laramide Orogeny, this entire sequence of sedimentary rocks was eroded from the top of the uplifted Beartooth block leaving only remnants of the Paleozoic sedimentary cover along some of the margins of the block.

Following the Laramide uplift, Tertiary and Quaternary volcanics, whose source is in Yellowstone National Park, blanketed the southwestern corner of the Beartooth Mountains. Also during the Quaternary, multiple glaciations occurred throughout the entire Middle Rocky Mountain region, including the Beartooth Mountains (Richmond, 1986).

GEOLOGY OF THE JARDINE AREA

Introduction

The bedrock geology of the Jardine area consists predominantly of Archean metasedimentary rocks that were intruded by granitic stocks and minor mafic dikes and sills. Greywacke and mudstone sequences have been regionally metamorphosed to quartz-biotite schist and biotite schist, respectively. The granitic stocks (e.g. the Crevice Mountain Stock) show no evidence of having been involved in the regional metamorphism that affected the metasedimentary rocks. Their age of emplacement, therefore, sets a latest age of 2600-2700 Ma for the regional metamorphic events that affected the metasedimentary rocks. The original thickness of the sedimentary pile is unknown, and a diamond drill hole on Mineral Hill (Figure 2), which was drilled to a depth of over 2000 ft., failed to intercept the crystalline basement beneath the sedimentary package. The thickness of the sedimentary pile has probably been exaggerated by tectonic thickening during an early episode of isoclinal, nappe-like folding. The monotonous nature of this thick pile of metasedimentary rocks is interrupted by a silicate facies iron formation which acts as the only stratigraphic marker horizon in the Jardine region.

The Archean metasedimentary rocks of the Jardine region are among the oldest rocks in the Beartooth Mountains. Dating of rocks in the Jardine-Crevice Mountain area was done first by Brookins (1968) and more recently by Montgomery and Lytwyn (1984).

Brookins (1968) reported a Rb-Sr age of 2660 ± 80 Ma for the emplacement of the Crevice Mountain quartz monzonite stock into the surrounding metasedimentary rocks. He further stated that the Crevice Mountain stock experienced a fairly strong metamorphic event about 1600 to 1800 Ma, and that the metasedimentary rocks are at least 2660 Ma old and may even be as old as 3300-3400 Ma.

Montgomery and Lytwyn (1984) confirmed Brookins data, reporting a Rb-Sr age of 2620 to 2760 Ma for the emplacement of the Crevice Mountain Stock. They suggest a resetting of biotite model ages by a regional thermal overprinting event at about 1800 Ma and report an age of approximately 3000 Ma for the metasedimentary rocks.

An age of 3200 Ma was determined from U-Pb dating of detrital zircons extracted from the metasedimentary rocks in the Jardine region (Mogk, 1988).

Lithologies

The metasedimentary rock types encountered during this investigation are quartz-biotite schist, intermediate-biotite schist, biotite schist, chlorite schist, and iron formation (grunerite schist). The nomenclature for the above rock types follows the convention currently in use at Mineral Hill Mine. Petrographic observations and references from earlier investigators pertaining to the lithologies in the region prove this naming scheme to be an accurate one. Previous investigators (Casella et al., 1982; Thurston, 1986) also include quartzite metaconglomerate and felsic metavolcanic rocks (quartz-

muscovite-plagioclase schist) as minor lithologies in the Jardine region.

Cliff-forming outcrops of diabase, usually in the form of a dike or sill with an average width or thickness of thirty feet, are the only intrusive igneous rocks seen in this field area. Some of the mafic dikes in the region, show an igneous texture that has been unaffected by tectonometamorphic events, while other mafic dikes (seen in underground exposures) are folded and intensely sheared in the metasedimentary package, indicating that they were included in the regional Precambrian deformational events. Also, previous investigators report Crevice Mountain granite crosscutting mafic dikes and mafic dikes crosscutting Crevice Mountain granite (Seager, 1944; Fraser et al., 1969; Casella et al., 1982). The mafic intrusions have not been dated, but the above observations indicate that some of the mafic dikes are older than the Crevice Mountain granite, while others are younger. The mafic dikes that are younger than the Crevice Mountain granite are at least Precambrian in age, since mafic dikes are not seen intruding Paleozoic or Mesozoic rocks (Fraser et al., 1969). The above observations suggest that a minimum of two generations of mafic igneous intrusions occurred in the region. All of the hills immediately surrounding Jardine, excluding Mineral Hill, are mantled by a thin Tertiary or Quaternary volcanic cover.

Low to medium grade (upper greenschist to lower amphibolite) regional metamorphism with a contemporaneous ductile deformational event caused the growth and preferential alignment of both matrix and porphyroblastic phyllosilicates in all of the

metasedimentary rocks in the area. This strong preferential alignment of micaceous minerals has created a schistosity which is along or nearly parallel to the original compositionally- and texturally-defined bedding planes.

A brief lithologic description of the rock types that are pertinent to this investigation follows. For a more comprehensive and detailed petrographic description of the Archean metasedimentary and igneous rocks in the Jardine area, the reader is referred to Seager (1944), Fraser, et al. (1969), Hallager (1980), and Thurston (1986).

Quartz-biotite schist is the dominant rock type in the region. In hand sample, it has a light greyish to brown color and distinct 0.5-2.0 mm "brown spots" of preferentially aligned biotite porphyroblasts in a matrix of fine- to medium-grained quartz and feldspar. This rock type is most often massive, but sometimes displays sedimentary structures such as grading or cross-bedding. The protolith of this rock type was a coarse-grained greywacke. Although the phyllosilicates (biotite, ± muscovite, ± chlorite) in the quartz-biotite schist exhibit a strong preferential alignment, their relatively small modal proportion (5-10%) in the rock shows, at best, a crude schistosity. Because this rock type lacks a pervasive foliation, it serves as a poor record for structural evidence of past Precambrian deformational events in the region.

Intermediate-biotite schist is the second most abundant rock type in the region. It differs from quartz-biotite schist by a decrease in quartz and feldspar grain size and an increase in the percentage of phyllosilicates in the matrix. This rock type is typically greyish in

color, fine-grained, and has an approximately equal ratio of biotite to quartz and feldspar. The micaceous minerals in the matrix are strongly preferentially aligned and wrap around biotite porphyroblasts, thus creating a domainal schistosity as defined by Marshak and Mitra (1988) (Figure 3). The protolith of this rock type is intermediate between greywacke and mudstone and probably tended towards a fine-grained, sandy- or silty-mudstone. At a few outcrop locations, this rock type displays a preferred mineral elongation direction in the plane of schistosity.

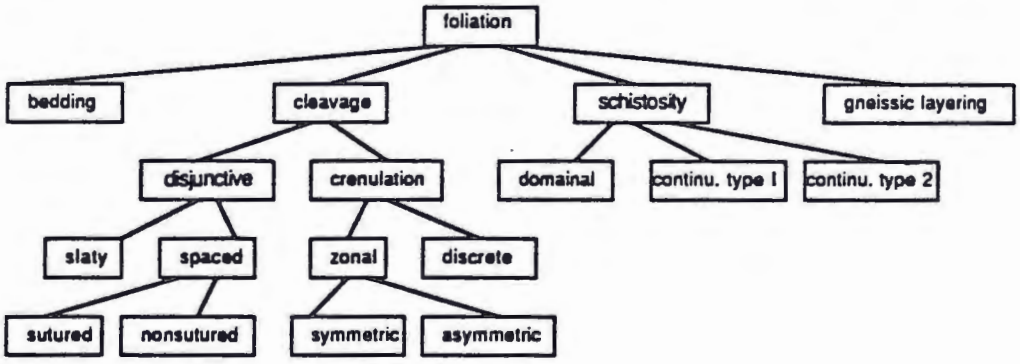

Figure 3. Flow chart for description of planar structures (From Marshak and Mitra, 1988, p. 243).

Biotite schist is not a common rock type in the region and is the rock type which best records structural evidence of Precambrian ductile deformational events. Biotite schist is usually brown to silver-grey in color with ≥ 25% mica, of which the majority is biotite. The protolith of the biotite schist was a mudstone. A very strong preferential alignment of phyllosilicate minerals and the lack of

anything larger than very fine-grained quartz, enhances a foliation of a form that has been defined by Marshak and Mitra (1988) as a continuous schistosity Type 1 (Figures 3 and 4).

Surface outcrops of iron formation in the Jardine region are scarce, but exposures can be found in prospect pits and adits since old time prospectors were aware that the lode gold in the region was associated almost exclusively with iron formation. Detailed subsurface mapping of iron formation on Mineral Hill has been accomplished through the use of both surface and underground diamond drill holes and face mapping during underground mining operations. Both silicate and oxide facies iron formation exist in the area with silicate facies iron formation being the more common of the two types.

Small pieces of magnetite-bearing banded iron formation in float on Bald Mountain and along Palmer Creek (Figure 2) were the only surface evidence of oxide facies iron formation in this study area. Airborne magnetometer survey data collected by the Anaconda Copper Mining Company (ACM) during the middle 1970's shows a regional magnetic high which has been interpreted by ACM to be a layer of oxide facies iron formation stratigraphically near the base of the metasedimentary rock package. This layer of iron formation has not been intercepted in the underground mine workings on Mineral Hill.

Silicate-facies iron formation is typically 1-10 meters thick, dark green to black in color, and displays 3-30 mm long radiating, bow-tie shaped amphiboles (grunerite and cummingtonite with retrograde

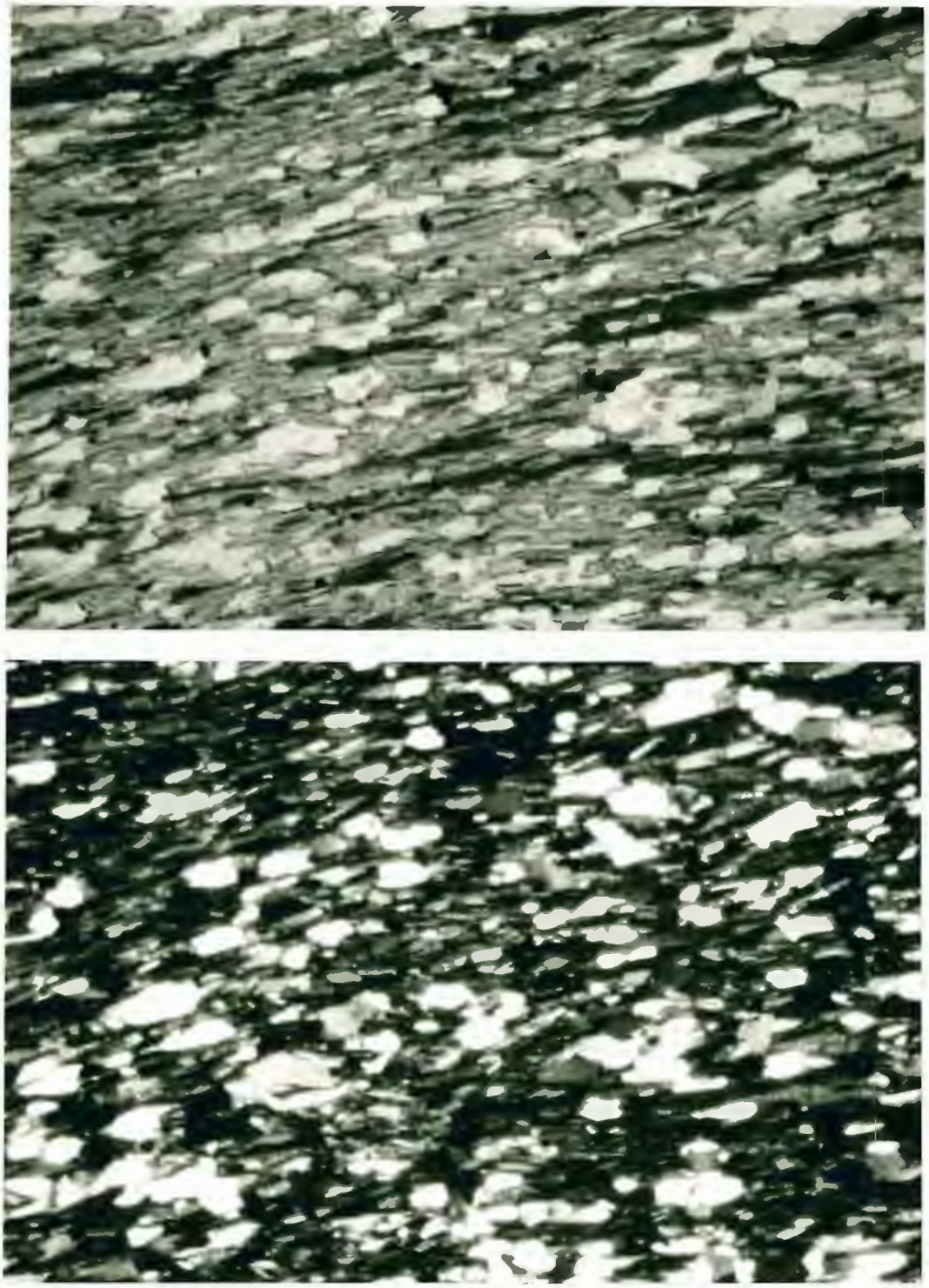

Figure 4. Photomicrographs of biotite schist, showing a continuous type 1 schistosity. Plane and crossed polarized light. Field of view is 2.5 mm by 1.7 mm.

hornblende). This facies of iron formation has a weak to moderate schistose fabric that is defined by the preferential alignment of the amphibole minerals (hence the name grunerite schist is used for this rock type by the mine geologists).

Chlorite schist, when found, is always in contact with iron formation. It has the same characteristics as biotite schist with the exception that chlorite is the dominant phyllosilicate in the rock. As one travels away from the iron formation, through the chlorite schist, a continuous gradation from chlorite schist to biotite schist may be found.

Garnet porphyroblasts may be found in all rock types but are most common in iron formation and chlorite schist. Microprobe data show that the garnets are almandine rich (X_{Alm} = 0.893). A dramatic increase in the occurrence of garnets in quartz-biotite schist was noted on Bald Mountain and is due to an increase in metamorphic grade eastward from Mineral Hill (discussed in more detail below).

Metamorphism

The metamorphic grade of the Archean metasedimentary rocks in the Jardine region is the lowest in all of the Beartooth Mountain Range (Mogk, 1988). From qualitative observations of rocks that contain coexisting staurolite, andalusite, garnet and chlorite, Thurston (1986) suggests a peak metamorphic pressure and temperature of 3.8 kb and 550°C.

A majority of the study area displays metamorphic mineral assemblages of biotite, muscovite, quartz, ± chlorite, ± garnet, and ±

feldspar. The lack of staurolite and/or an aluminum-silicate mineral in this assemblage suggests that most of the study area lies below the staurolite isograd.

Surface evidence for a staurolite isograd was found between Mineral Hill and Bald Mountain (Figure 2). Outcrops on Mineral Hill display metamorphic mineral assemblages typical of zones below the staurolite isograd, while samples found on Bald Mountain show the first occurrence of staurolite and aluminum-silicates and also show an increase in the number of garnets per unit volume of rock. Since outcrop exposure in the area is limited, a staurolite isograd between Mineral Hill and Bald Mountain can only be located approximately.

Evidence of a staurolite isograd has also been reported in core from a diamond drill hole that was drilled at an azimuth of 270° with an inclination of 78°, into the top of Mineral Hill. Diamond drill hole J-71, with a collar elevation of 7534 feet, shows a first occurrence of staurolite at a drill-hole distance of 2032 feet (equal to an elevation of approximately 5550 feet) (Homestake Mining Company thin section J71-2032). The staurolite prisms seen in thin section J71-2032 are identical in size, freshness, and habit to those seen in the Bald Mountain samples.

Two samples from Bald Mountain proved to be valuable for the analysis and calculation of a metamorphic pressure and temperature of the rocks in the study area. Although the samples were collected as float rather than from outcrop, this author believes that they are representative of bedrock proximal to their collection location.

Sample BM-2 has a metamorphic mineral assemblage of biotite, garnet, staurolite, and quartz, without muscovite (Figure 5A). An analysis of this sample could be used only as a geothermometer since it lacked muscovite and an aluminum-silicate mineral. Sample BM-3 has a metamorphic mineral assemblage of biotite, staurolite, andalusite, sillimanite, muscovite, and quartz (Figure 5B). Both pressure and temperature of metamorphism could be calculated using the BM-3 sample analysis.

Analytical Procedure

Polished thin sections of samples BM-2 and BM-3 were prepared for analyzing the compositions of coexisting metamorphic minerals. Mineral compositions were determined using the electron microprobe at the Natural Resources Research Institute in Duluth, Minnesota. Coexisting biotite, garnet (which showed no Fe or Mg zoning), and staurolite were probed in sample BM-2, and coexisting biotite and staurolite were probed in sample BM-3. Compositions and formulas of the minerals probed in these two samples can be found in the Appendix.

Pressure-temperature phase diagrams for both samples were calculated by entering mineral activity data into the software package, GE0-CALC (Berman et al., 1987; Perkins et al., 1986; Berman et al., 1985). Using the exchange reaction

almandine + phlogopite $\Leftrightarrow$ pyrope + annite (1)

and mineral composition data from sample BM-2, a temperature of metamorphism was calculated. The position of the reaction

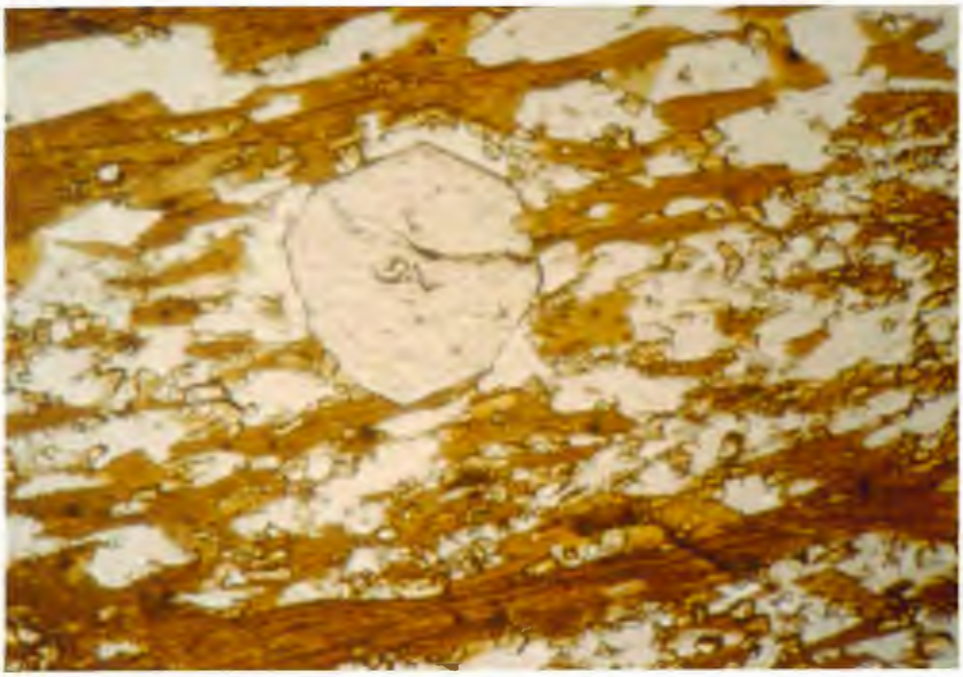

A

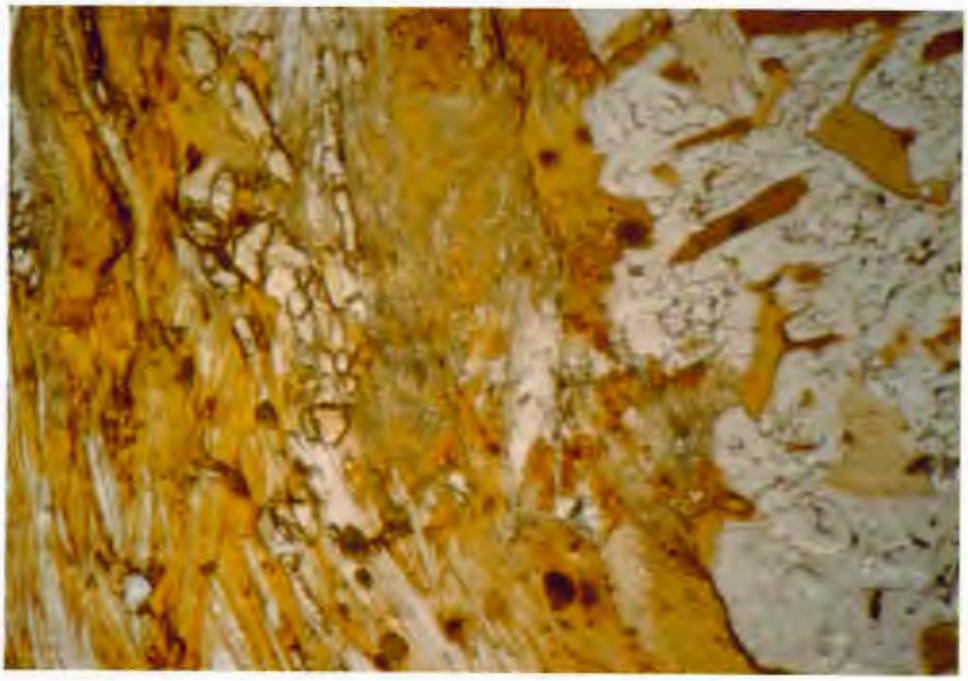

B

Figure 5. Photomicrographs of: A) Sample BM-2 and B) Sample BM-3. Both are shown in plane polarized light with a field of view of 2.5 mm by 1.7 mm.

annite + quartz + staurolite ⇔ almandine + muscovite + water (2)

was also calculated to see if it would intersect the exchange reaction (1) and thus give a limiting pressure for sample BM-2. This did not provide any useful constraint.

Using mineral composition data from sample BM-3, the reactions

Fe-staurolite + quartz + muscovite ⇔ andalusite + annite + water (3)

Fe-staurolite + quartz + muscovite ⇔ sillimanite + annite + water (4)

andalusite ⇔ sillimanite (5)

were used to calculate a pressure and temperature of the system. Calculations of exchange reactions between Fe- and Mg-staurolite could not be performed because thermodynamic data for Mg-staurolite is currently unavailable.

Results

Figure 6 shows the reactions for samples BM-2 and BM-3 in pressure and temperature space. The temperature of metamorphism calculated from sample BM-2 data, using reaction (1), is approximately 490°-500°C. The pressure and temperature of metamorphism calculated from sample BM-3 data, using reactions (3), (4), and (5), are approximately 2.9 kb and 560°C.

The metamorphic mineral assemblages that were analyzed with the microprobe, show evidence of being either syn- or post-F_1 but pre-F_2. In other words, the reported pressure and temperature of metamorphism are representative of conditions that existed during or shortly after the first phase of folding.

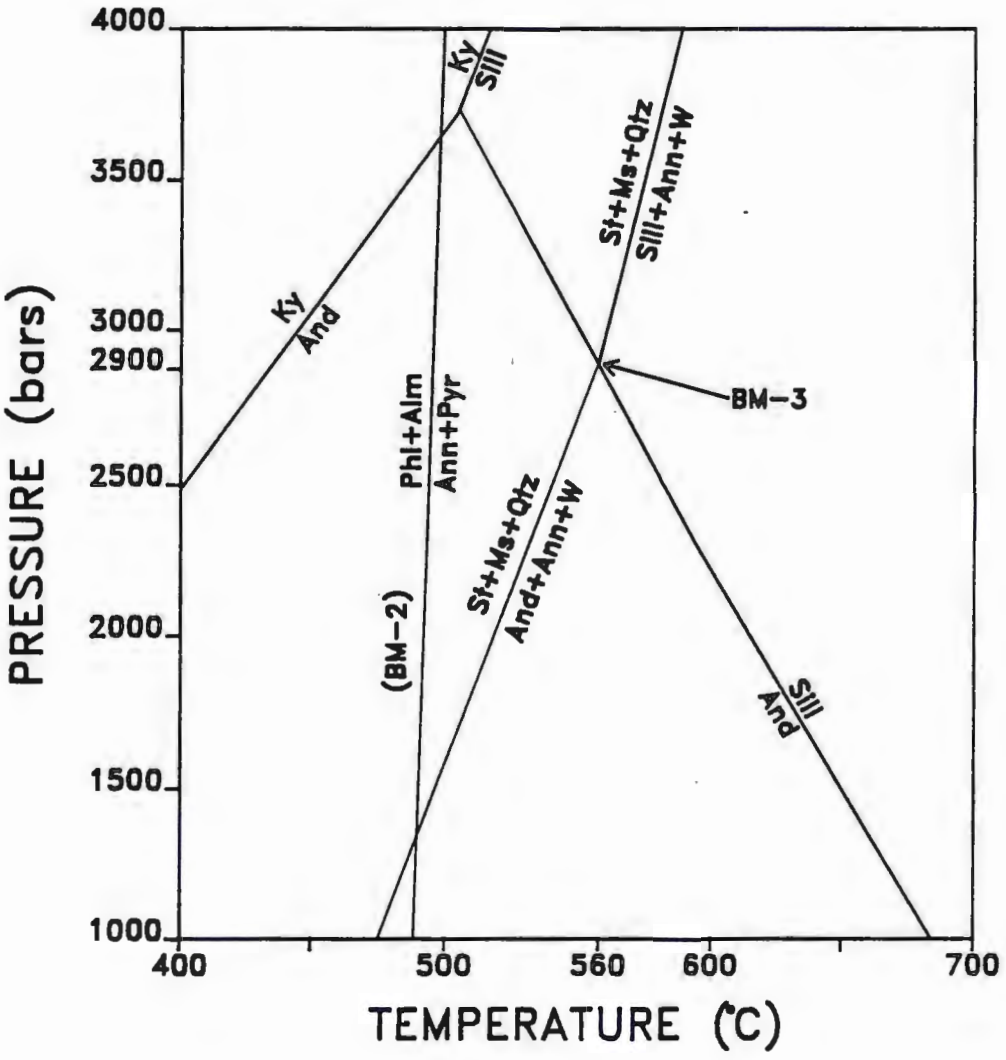

Figure 6. Pressure and temperature phase diagram showing the reaction boundaries representative of samples BM-2 and BM-3 along with the aluminum-silicate reactions boundaries.

The accuracy of the reported pressure and temperature of metamorphism using sample BM-3 is dependent on the positioning of the andalusite-sillimanite reaction in pressure-temperature space. The position of the andalusite-sillimanite reaction is not well constrained because the free energy value for this reaction has a high degree of uncertainty (169 ± 194 cal/mol at 750°C and 1 atm; Deer, Howie, and Zussman, 1982). Also, the transition between these two aluminum-silicate polymorphs is slow, allowing a metastable polymorph to exist in the stability field of the other polymorph (Deer, Howie, and Zussman, 1982).

The discrepancy of 60°C between the two calculated closure temperatures (the temperature at which exchange reactions stop) may be due to varying rates of divalent cation exchange between Fe and Mg in the garnet and biotite during reequilibration of those metamorphic minerals with changing pressure and temperature conditions. Sample BM-3 may represent the closure temperature of metamorphic culmination, while sample BM-2 may represent a retrograde closure temperature. The closure temperature discrepancy may also be due to a small analytical error in sample BM-2 microprobe data. Spear and Peacock (1989) report that with an analytical error of ±3-5%, the accuracy of an Fe-Mg exchange thermometer is within approximately ± 30-50°C.

Figure 7 is the petrogenetic grid of Spear and Cheney (1989) for the KFMASH system. Overlain on the grid are contour lines (isopleths) for X_{Alm} (Fe/Fe+Mg) for a system with garnet + biotite.

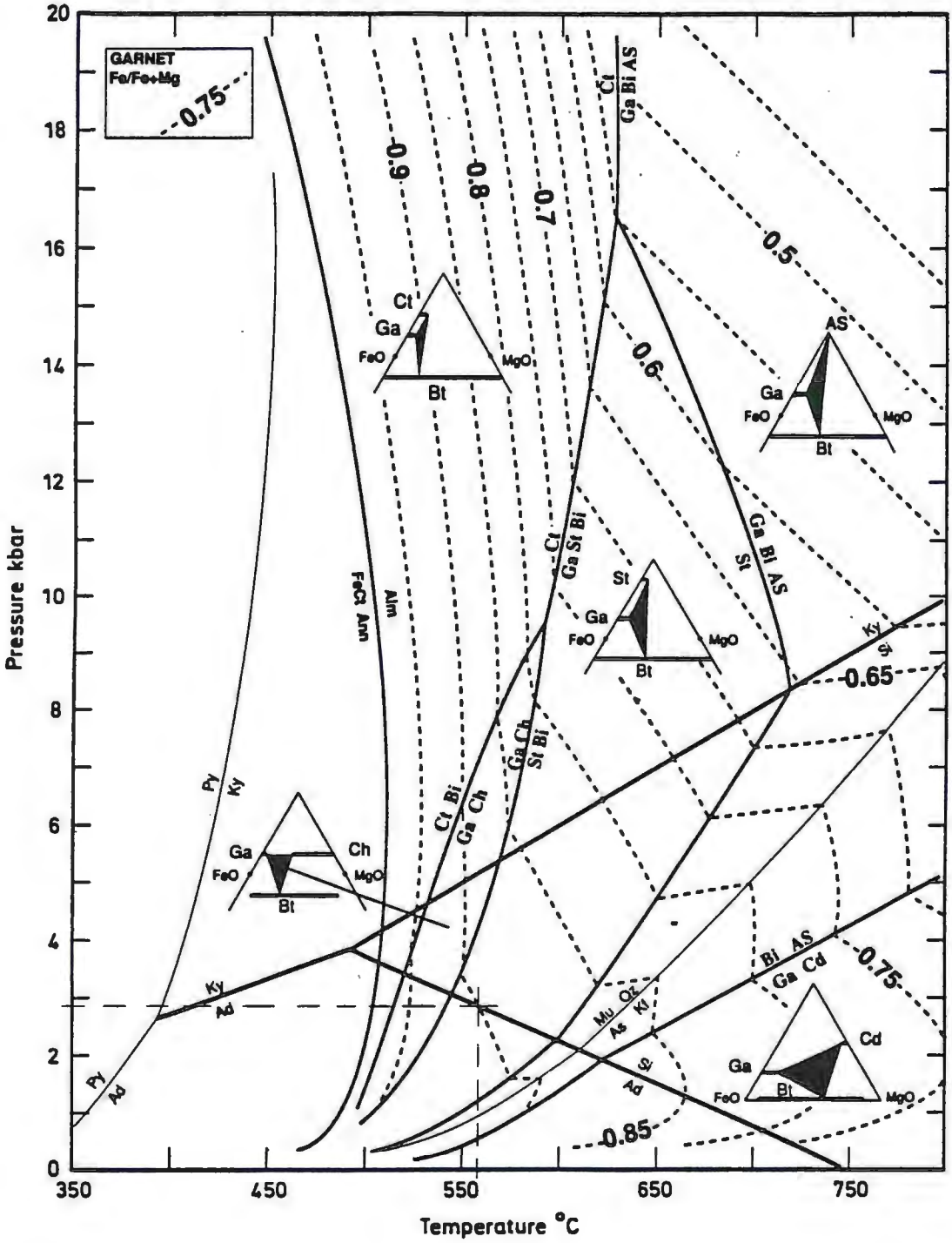

Figure 7. Petrogenetic grid for the KFMASH system (From Spear and Cheney, 1989)

According to Spear and Peacock (1989), iron is partitioned between garnet and biotite. The assumption made here is that the composition of the garnets (X_{Alm} = 0.893) coexisting with biotite in sample BM-2 represent a maximum X_{Alm} composition of garnets in an assemblage of quartz-muscovite-garnet-biotite-staurolite that is isofacial with sample BM-3. This assumption can be substantiated by comparing the mole fraction of iron in biotite for samples BM-2 (X_{Fe} = 0.539) and BM-3 (X_{Fe} = 0.532) and noting that the difference between the two samples is insignificant.

Using the composition of the garnets in sample BM-2 (X_{Alm} = 0.893), the 0.9 X_{Alm} isopleth will be followed in figure 7. The segment of the 0.9 X_{Alm} isopleth that is pertinent to the BM-2 and BM-3 metamorphic mineral assemblages lies in the field between the reactions

$$\text{garnet} + \text{chlorite} \Leftrightarrow \text{staurolite} + \text{biotite} \qquad (6)$$

$$\text{staurolite} \Leftrightarrow \text{garnet} + \text{biotite} + \text{Al-silicate} \qquad (7).$$

The 0.9 X_{Alm} isopleth, in the field defined above, crosses reaction (5) at approximately 2.9 kb and 560°C (see Figure 7). This agrees well with the pressure and temperature calculated from sample BM-3. At this pressure and temperature, the metamorphic mineral assemblage garnet + biotite + staurolite (sample BM-2) and biotite + staurolite + andalusite + sillimanite (sample BM-3) are stable and may coexist (Figures 7 and 8).

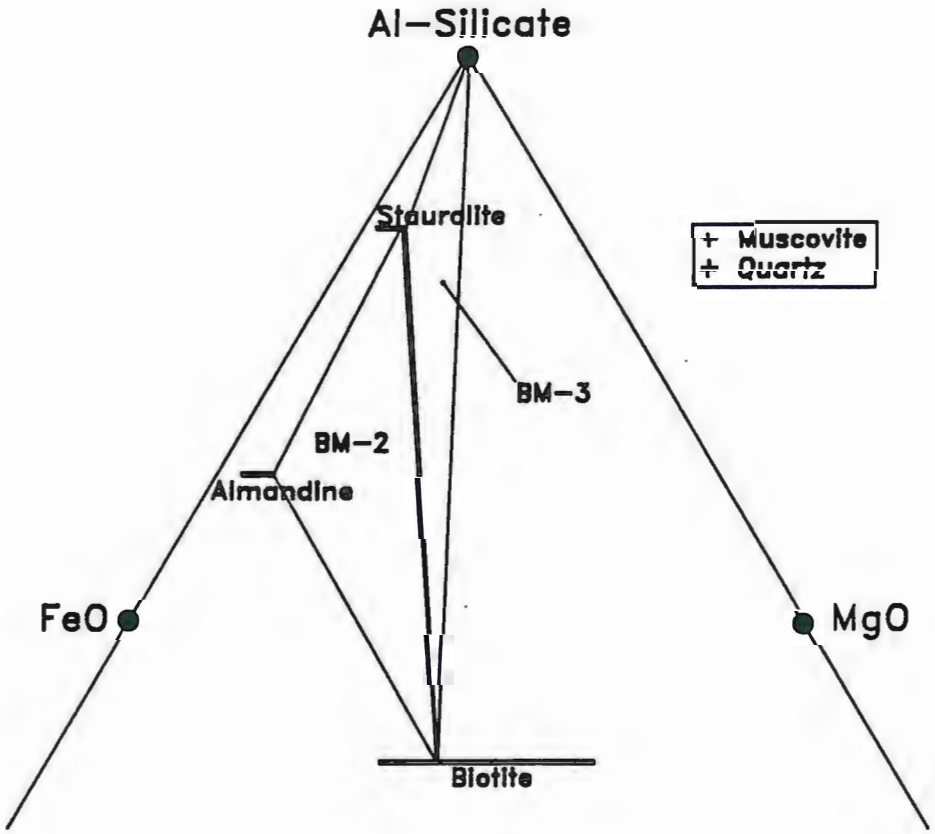

Figure 8. AFM diagram showing coexisting metamorphic mineral assemblages for samples BM-2 and BM-3.

Descriptive Structural Geology

Introduction

Evidence for three generations of folding has been recognized in the Archean metasedimentary rocks of the Jardine region. Correlation of fold generations across the region was accomplished using the distinct styles and consistent orientations of minor structures. Through structural features in surface and underground outcrops, it can be shown that each generation of folding was unique and separate from the preceding or succeeding fold event(s).

The Crevice Mountain stock, approximately 4 km southeast of Jardine, shows no evidence of having had experienced a regional deformation after its emplacement. Therefore, the age of the ductile deformations experienced by the metasedimentary rocks has been constrained by the age of the emplacement of the Crevice Mountain stock (2620-2760 Ma; Montgomery and Lytwyn, 1984).

Structural Elements

Planar and linear structures from surface outcrops were measured and used to calculate the shapes and orientations of the three fold events. Planar structures measured include a pervasive schistosity and two generations of crenulation cleavages. Linear structures measured include minor fold axes, lineations defined by the intersection of two planar structural elements, and a mineral lineation.

Planar Structures

The most prominent planar feature in the region is a ubiquitous foliation, here designated S_1. This foliation plane is the result of metamorphic and tectonic processes, which together promoted the growth and preferential alignment of coarse-grained micaceous minerals parallel to the axial surface of the first generation of folding (F_1). Where bedding and S_1 could be observed in the same outcrop, S_1 was parallel or nearly parallel to bedding planes (S_0). S_1 was never found crossing bedding planes at a high, or even moderate angle. Using the terminology of Marshak and Mitra (1988, p. 243), the S_1 foliation is classified as a continuous schistosity Type 1 (Figure 3).

A few outcrops were found in which the S_1 foliation was defined by a metamorphic layering (Figures 9A and 9B). These samples display mica-rich domains (0.5-2.0 mm thick) in which the layer silicates show a strong preferential alignment, separated by quartz-rich microlithons (0.5-2.0 mm thick; Figure 9B). Dissolution, migration, and redeposition of quartz from the mica-rich domains to the quartz-rich microlithons, along with reorientation of the micaceous minerals in the domains, occurs in response to applied stresses (Williams, 1972; Hobbs et al., 1976; Gray and Durney, 1979). The mechanism that drives the diffusion of the dissolved minerals is thought to be a normal-stress controlled variation in chemical potential in a stressed anisotropic fabric (Gray and Durney, 1979).

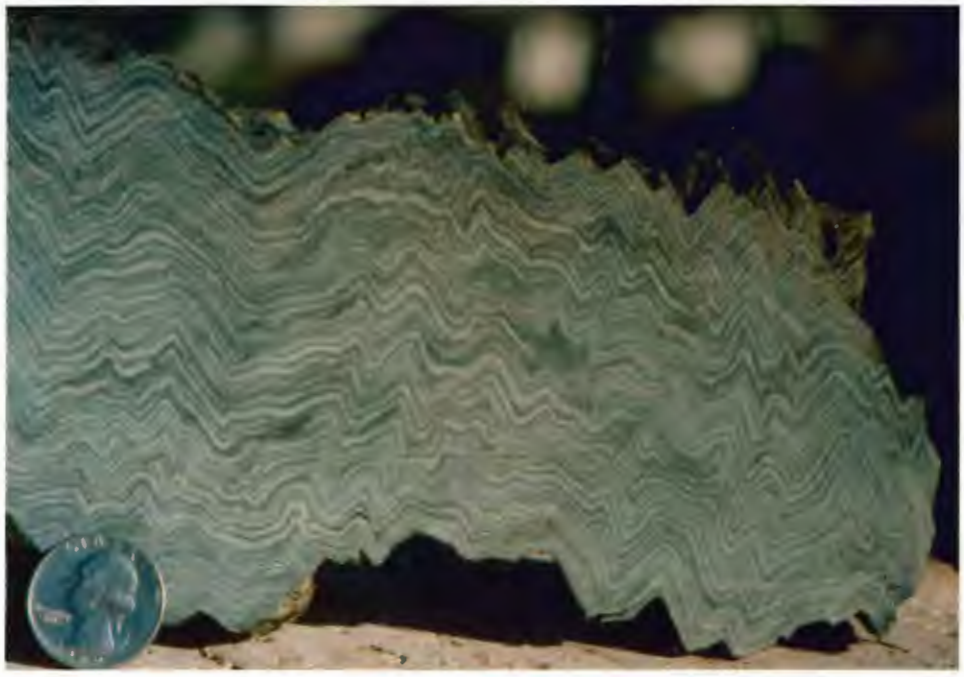

A

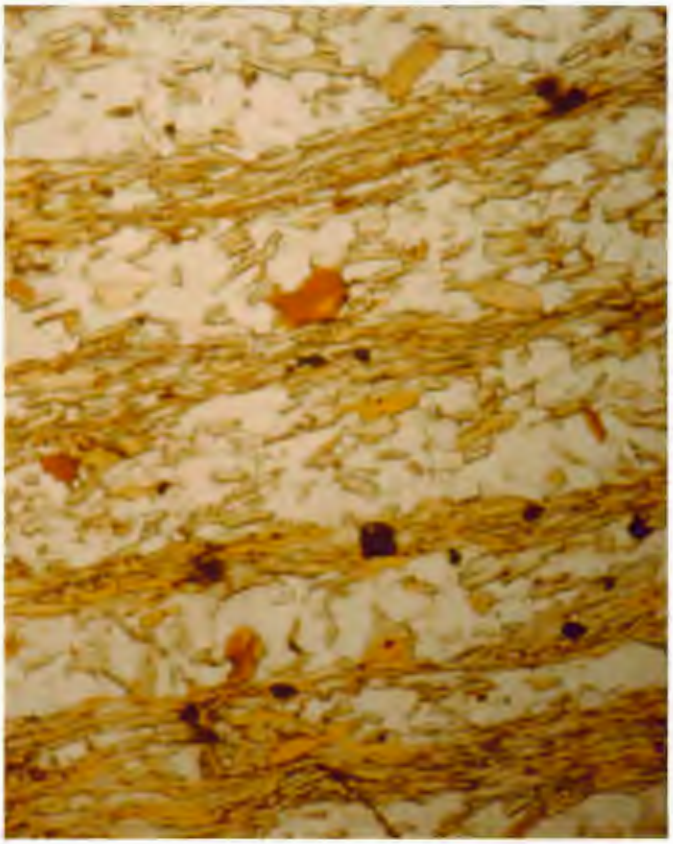

B

Figure 9. Metamorphic layering of S_1 as seen in: A) Hand sample where S_1 is crenulated and B) Thin section. Photomicrograph field of view is 2.5 mm by 1.7 mm.

Other planar features include foliations that are crenulation cleavages of S_1, formed during, and in axial-planar attitudes to, the second (F_2) and third (F_3) fold events. These crenulation cleavages are designated S_2 and S_3, respectively, and are both a zonal crenulation cleavage (Marshak and Mitra, 1988, see Figure 3), defined by the axial planar alignment of microfold hinges (symmetric zonal crenulation cleavage; Figure 10A) and/or domains of reoriented micas (asymmetric zonal crenulation cleavage; Figure 10B) and are not the result of recrystallization of micaceous minerals in the microfold hinges during tectonometamorphic processes. Thin section observations show that the micaceous minerals that define S_1 are bent and/or kinked into microfolds with hinge lines that are in alignment parallel to the axial planes (S_2 and S_3) of later fold generations (Figure 10, A and B). When both sets of axial-planar crenulation cleavages were observed in a coexisting fold hinge (a dome), the amplitude of the microfolds that define the S_2 crenulation cleavage were typically larger than the amplitude of the microfolds in the S_3 crenulation cleavage. This has been interpreted to be the result of varying relative intensities of the F_2 and F_3 fold events, in agreement with mesoscopic observations of F_2 and F_3 folds.

The limbs of asymmetric microfolds are composed primarily of micaceous minerals, while the hinges of asymmetric microfolds show an excess of quartz (Figure 10B). Nicholson (1966), Williams (1972), Cosgrove (1976), Hobbs et al. (1976), Marlow and Etheridge (1977),

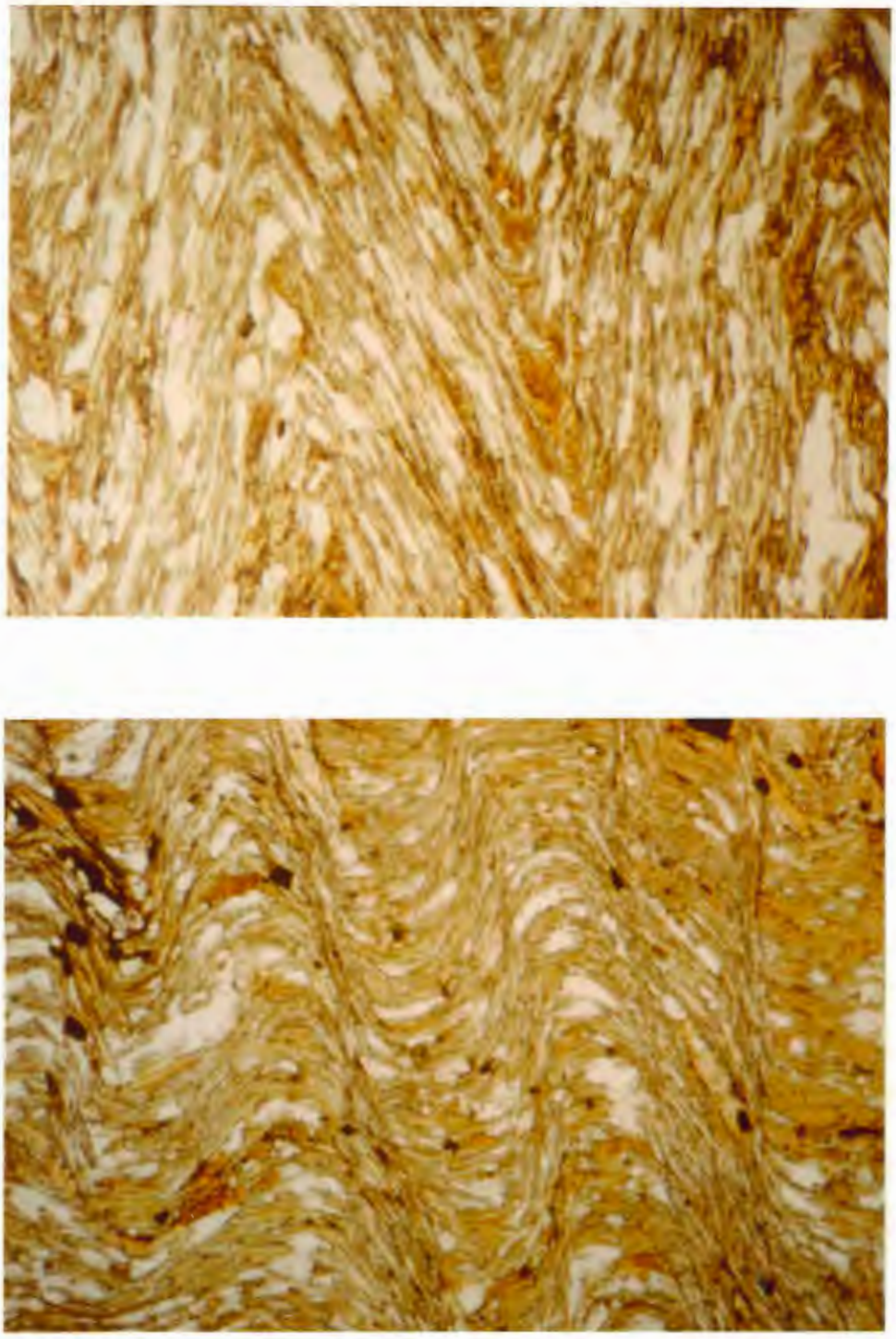

Figure 10. Photomicrographs of: A) Symmetric zonal crenulation cleavage and B) Asymmetric zonal crenulation cleavage. Both are in plane polarized light and field of view is 2.5 mm by 1.7 mm.

and Gray and Durney (1979) report that the process responsible for the formation of differentiated crenulation cleavage (Marshak and Mitra's asymmetric zonal crenulation cleavage) is the dissolution of soluble minerals (i.e. quartz) at the microfold limbs with migration and redeposition of the dissolved material at the microfold hinges. The migration of the dissolved mineral species is driven by a chemical potential gradient, which is itself, due to a differential normal stress in the fabric of the rock (Gray and Durney, 1979). This is illustrated in figure 11, taken from Gray and Durney (1979).

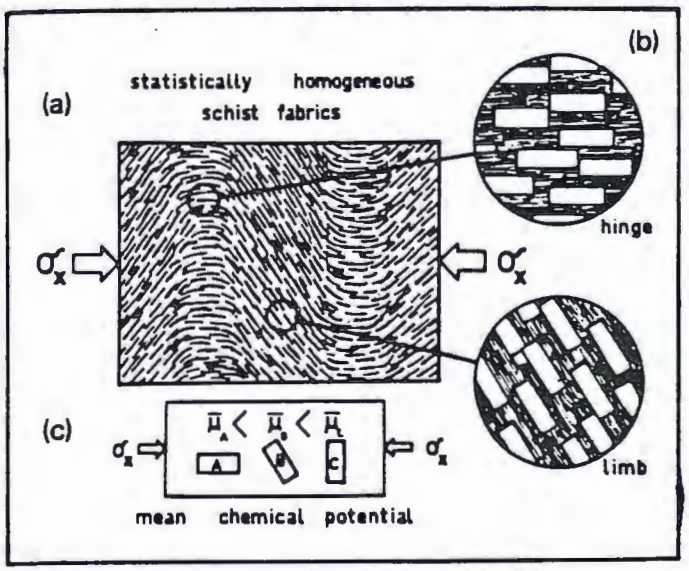

Figure 11. (a) Mineral shape and orientation in a differentially stressed anisotropic fabric. (b) Inserts show the orientation of minerals in the limb and hinge of a microfold. (c) Variation of the mean chemical potential of grains with different orientations with respect to σ_x (From Gray and Durney, 1979).

Kink bands were observed at two locations in the study area. They are defined by a sharp deflection of the S_1 schistosity, usually

across a small (cm scale) domain. A small outcrop on Germania displayed a 2 cm wide kink band with a northeast-southwest strike and a moderate dip to the northwest. Although this kink band has a strike similar to that of S_2, it has a fundamentally different geometry than F2 folds (discussed below), and cross-cutting structural features show that it was not developed during, but rather later than, the F_2 phase of folding. A large (0.4 m wide), nearly horizontal kink band was also seen at the confluence of Bear Creek and the Yellowstone River. The kink bands are a rare structural feature, and observations of the two mentioned show that they deform earlier structural features. The kink bands are therefore interpreted to be part of a post-F_3 deformational event.

Linear Structures

Three types of lineation are found in the metasedimentary rocks of the Jardine region: minor fold axes, intersection lineations, and a mineral lineation.

Minor fold axes were observed in surface outcrops of all rock types. The minor fold axes that were recorded from surface exposures were most often associated with the second generation of folding (F_2). A few F_3 fold axes were observed in outcrop but could not be measured directly due to the weak nature of the third fold event. Distinct F_1 minor fold axes were never found in surface exposures, but they were observed underground. The amplitude of F_2 minor folds that were observed on the surface ranges in size from approximately 5.0 centimeters up to 10 meters. F_2 folds with large

amplitudes were also observed in underground exposures in Mineral Hill.

Intersection lineations are the most common of the three types of lineation and were found most often in outcrops of intermediate-bioitite schist and biotite schist. The intersection of well-developed S_2 and/or S_3 axial planar crenulation cleavages with the S_1 foliation plane results in an intersection lineation on the S_1 surface (Figure 12). Depending on the intensity of the crenulation cleavage, an intersection lineation usually gives the S_1 surface a corrugated appearance (Figure 12). The amplitude and wavelength of microfolds that define the intersection lineation range from millimeter-scale to centimeter-scale and are almost always symmetric in shape. The intersection lineations were formed during the F_2 and F_3 fold events and are here designated L_2 and L_3, respectively. L_2 lineations are more prevalent and more prominent than L_3 lineations, which are always less well-developed and occur more infrequently than L_2 lineations. Outcrops that display both L_2 and L_3 lineations are rare. At such locations, L_2 and L_3 are at a moderate to high angle to one another.

A mineral lineation, defined by the preferential alignment of biotite porphyroblasts, can be seen in the S_1 foliation plane in a few outcrops of intermediate-biotite schist. Figure 13 is a stereoplot of the orientation of observed mineral lineations along with L_2 and L_3 lineations for comparison. The stereoplot shows that the mineral lineation is not colinear with either L_2 or L_3 lineations.

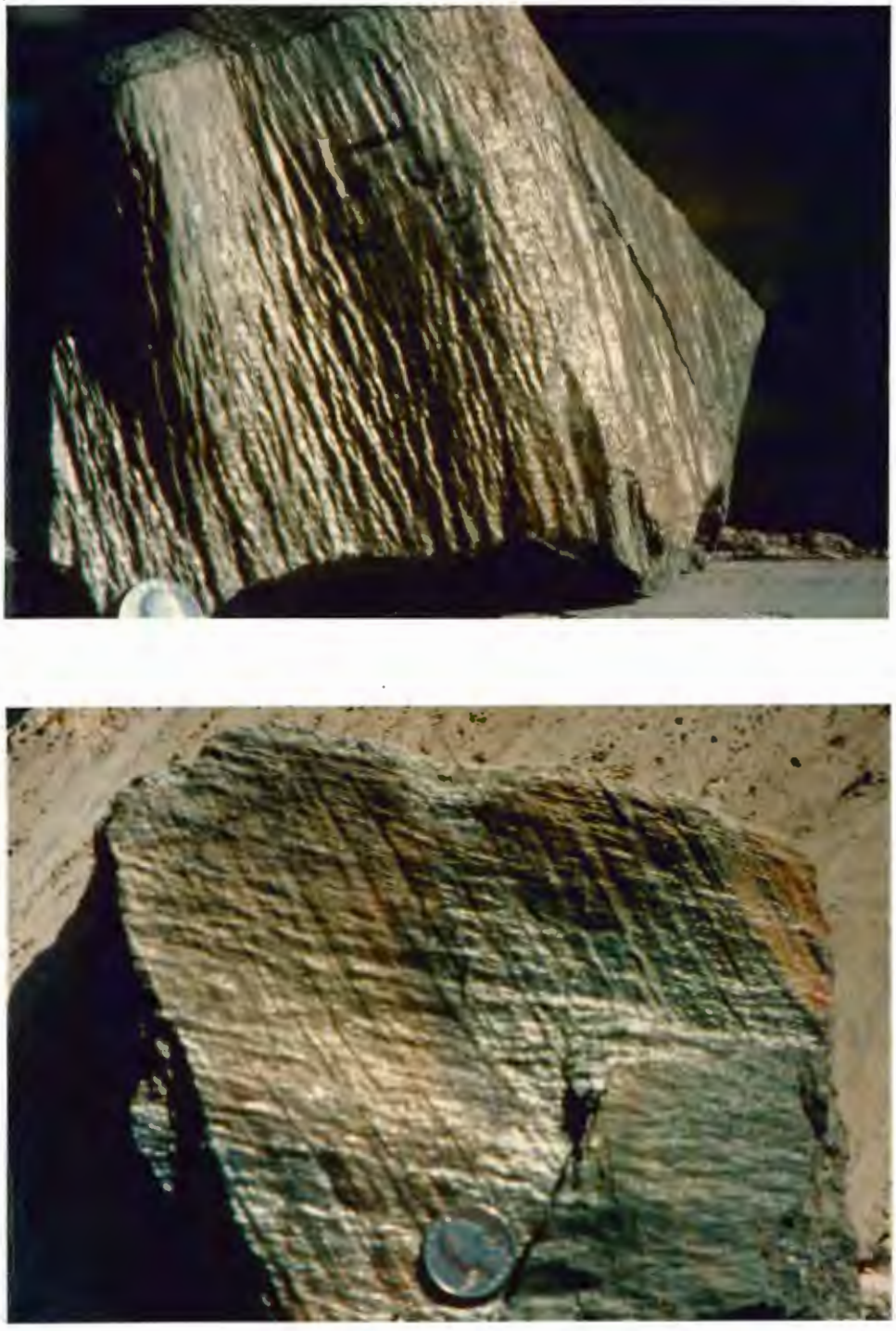

Figure 12. Hand samples showing L_2 and L_3 intersection lineations on S_1. In the upper photograph, L_2 is nearly vertical and L_3 is nearly horizontal. In the lower photograph, L_2 and L_3 are not differentiable.

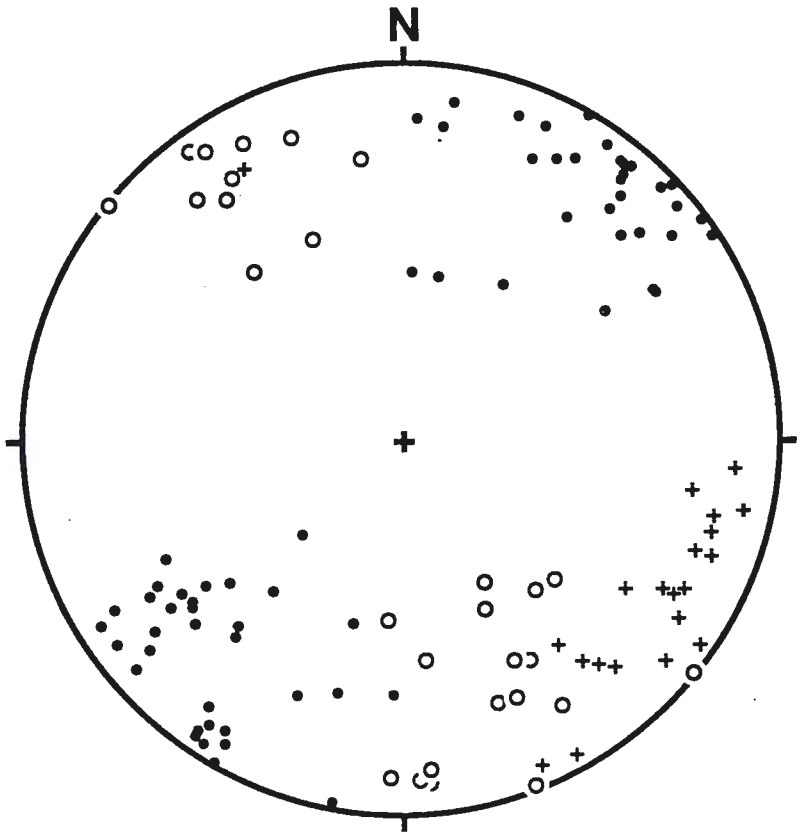

Figure 13. Stereoplot showing compilation of regional lineation data (not including F_2 fold axes). Filled circles are L_2, open circles are L_3, and crosses are mineral lineations.

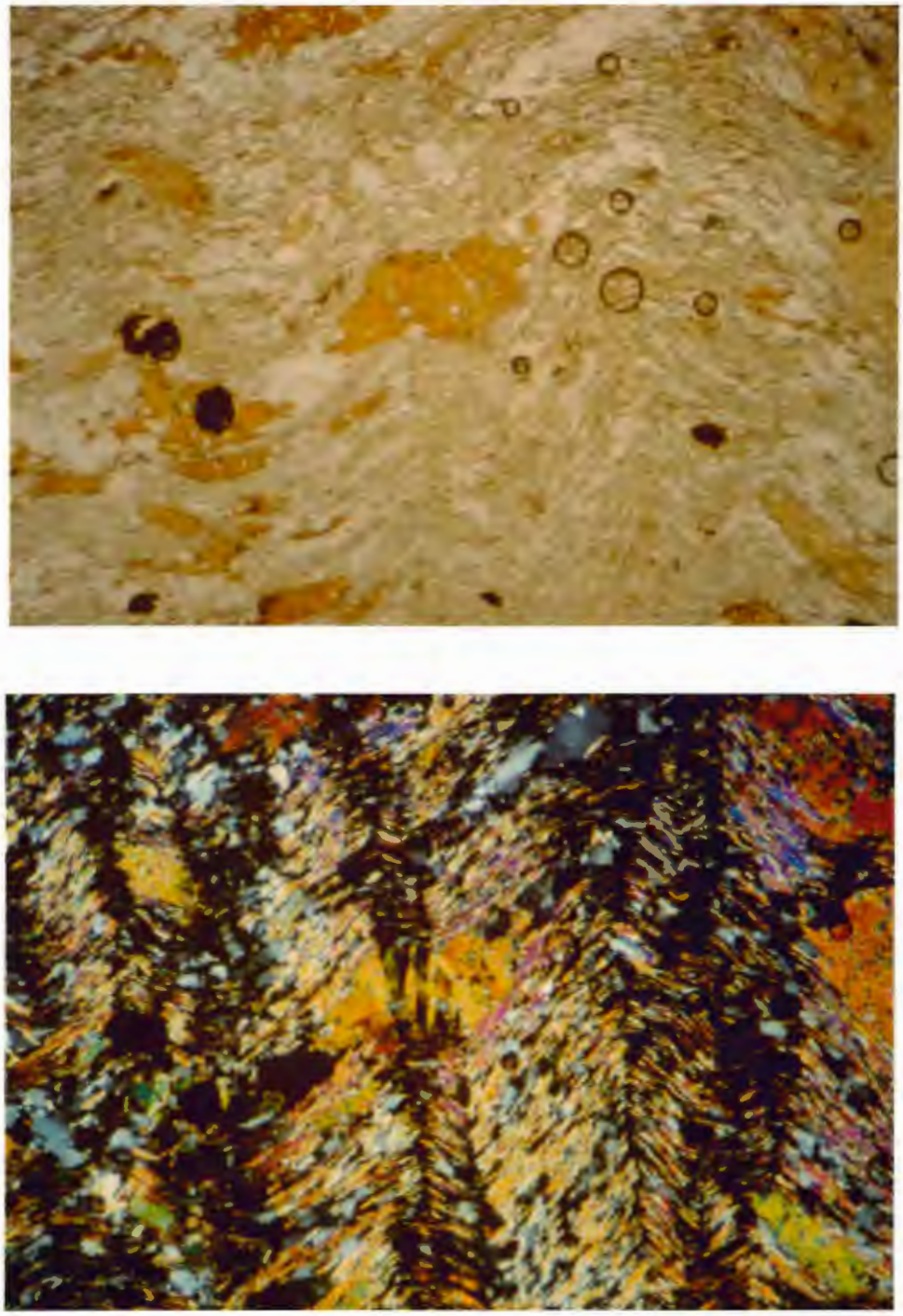

Figure 14. Photomicrographs of biotite porphyroblasts bent and kinked in S_2 crenulation cleavage. Upper photograph is in plane-polarized light, lower photograph is in cross-polarized light. Field of view for both is 2.5 mm by 1.7 mm.

Thin section evidence, in the form of bent and kinked biotite porphyroblasts (Figure 14), shows that the biotite porphyroblasts that define the mineral lineation are at least pre-F_2 and may possibly be pre- or syn-F_1. Since the biotite porphyroblasts are not likely to have a detrital origin, they are probably the result of a tectonometamorphic recrystallization process that occurred before, during, or shortly after the F_1 fold event. The number of outcrops displaying a mineral lineation is small, and nowhere in the study area was an outcrop found in which the mineral lineation had an obvious association with a structure of any generation. It is therefore concluded, that a structural significance of the mineral lineation to any fold event cannot be confidently determined at this time.

Geometry of Individual Folds

The three generations of folding recognized in the Jardine region are herein labeled, from earliest to latest, F_1, F_2, and F_3. Each generation of folding has characteristic minor structures (defined above) that were used to determine their shape and orientation.

F_1 Folds

Folds developed during the first generation of folding (F_1) are isoclinal (interlimb angle equals 0° to 10°) and likely were recumbent at the time of their formation, but have been affected by later refolding. F_1 fold hinges were not observed in surface outcrop, but minor F_1 fold hinges were observed in underground exposures in

the Mineral Hill Mine. As expected, the hinge zones of large-scale isoclinal folds are rarely seen because the majority of the fold surface is fold limb rather than fold hinge. The F_1 minor folds seen underground are typically tabular shaped, isoclinally folded quartz bodies 2-40 cm thick, or isoclinally-folded bands of massive sulfide (arsenopyrite) in iron-formation (Figure 15).

The large-scale isoclinal nature of F_1 folding is demonstrated well in cross-section interpretations of iron formation locations in Mineral Hill. With surface and underground diamond drill holes, the iron formation can be accurately located and mapped (Figure 16). By using the iron formation as a marker horizon, it can be seen that the iron formation has been isoclinally folded during the first phase of folding (F_1) and subsequently refolded by a later phase of folding (in this cross section, F_1 is refolded by F_2) (Figure 16).

The coplanarity of bedding and S_1 foliation, seen in the surface outcrops throughout the region, has been interpreted as evidence that the first fold event was isoclinal. Minor F_1 folds underground display an axial-planar schistosity (S_1) that corroborates this interpretation and dispels any notion that the S_1 foliation is the result of a relict primary sedimentary texture of preferentially oriented micas.

Figure 17A is a stereoplot of poles to the S_1 foliation measured from surface outcrops throughout the region. The apparent random scatter of S_1 orientations, as displayed in the plot, is the result of the S_1 surface being deformed by two later generations of folding (F_2 and F_3).

Figure 15. F_1 fold observed in underground exposure in Mineral Hill Mine.

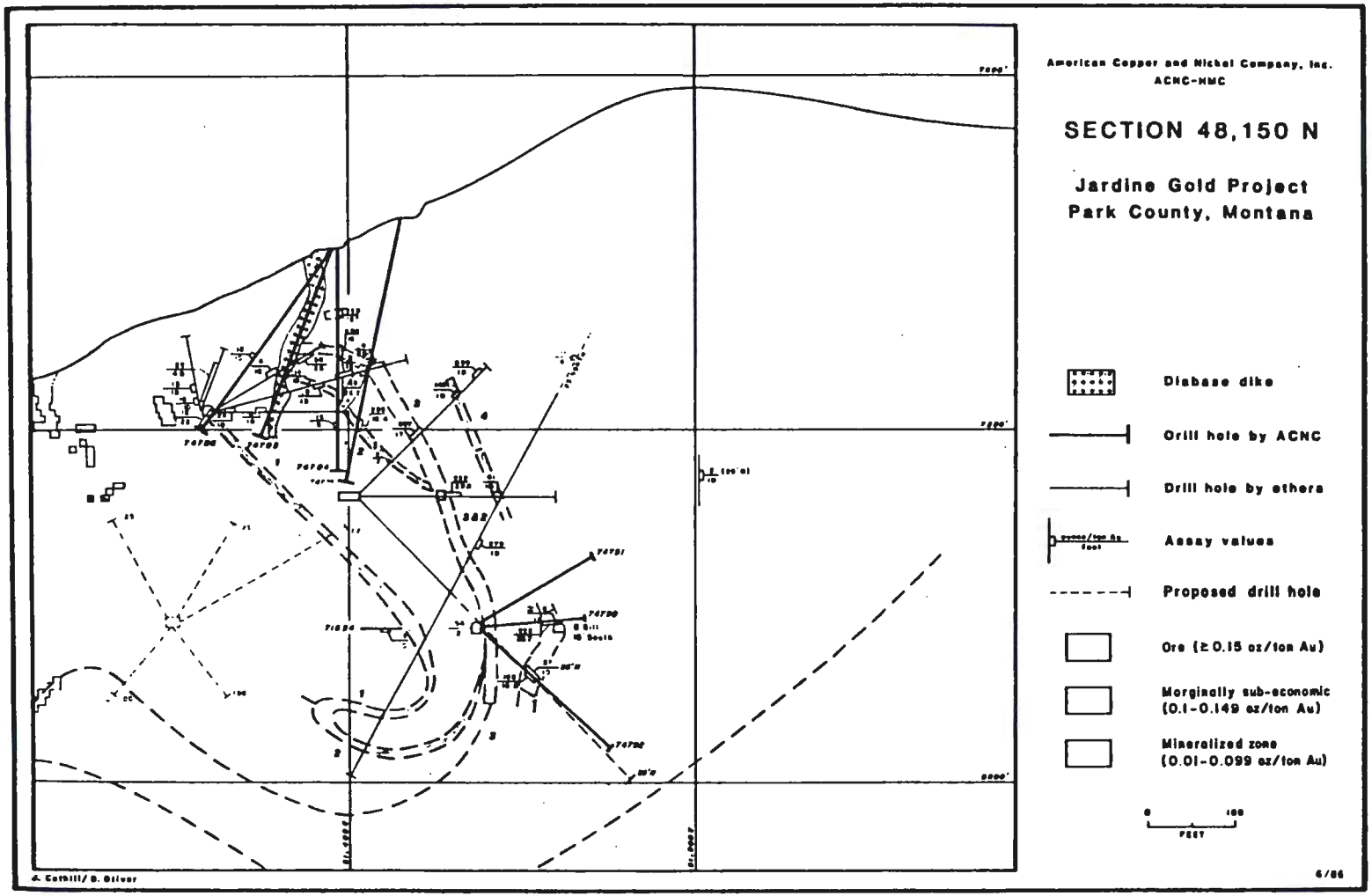

Figure 16. Cross section through Mineral Hill showing large-scale, multiply folded iron formation (From ACNC).

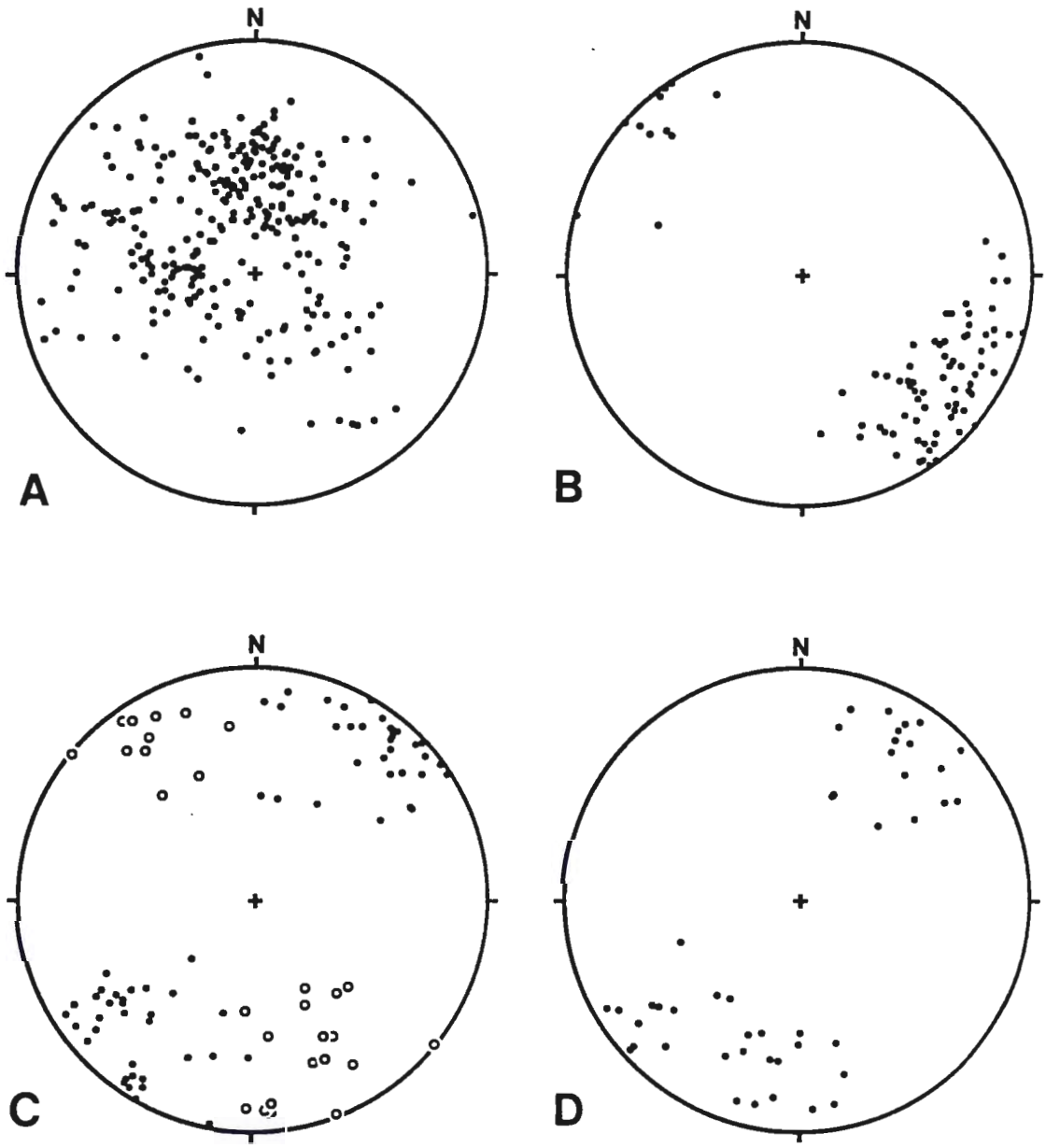

Figure 17. Stereoplots showing compilation of planar and linear minor structures. A) Filled circles are poles to S_1. B) Filled circles are poles to S_2. C) Filled circles are L_2, open circles are L_3. D) Filled circles are F_2 fold axes.

Measurements of the orientation of minor F_1 fold hinges were not collected because the underground exposures were always two-dimensional and the structures discontinuous. Underground mapping by the Mineral Hill Mine geologists shows that F_1 fold axes show no preferential orientation, and in fact, can be found to occur in almost any direction and with any degree of plunge (personal communication with David Oliver). There are two reasons for the omnidirectional nature of the F_1 fold axes. First, the shape of F_1 folds before deformation was noncylindrical with an undulatory hinge line; that is, F_1 fold morphology closely resembled the morphology of sheath folds. Second, F_1 hinge lines were deformed and reoriented by two successive fold generations.

F_2 Folds

The second generation of folds (F_2) is cylindrical and close (interlimb angle equals 30° to 70°), with subhorizontal to moderately plunging fold axes and nearly upright axial surfaces. The axial surface of the second generation of folds, as evidenced by measurements of S_2 crenulation cleavages and L_2 lineations on S_1 foliation planes, strikes northeast-southwest (average strike = 055°) and dips steeply (60°-90°) to the northwest and sometimes to the southeast (Figures 17B and 17C). Measurements of fold axes show that F_2 fold hinges plunge gently to the northeast (≈ 030°) or to the southwest (≈ 210°) (Figure 17D).

The doubly-plunging nature of the F_2 fold axes is attributed to subsequent deformation of the hinge lines by the third generation of

folding. The fold axes of the second and third fold event are at a high angle to each other and the axial surface of the second generation of folding shows no evidence of deformation (buckling) by the third generation of folding, as the direction of displacement of the third generation of folding lies within the axial surface of the second generation of folding. The subject of superposition of fold generations is covered in more detail below, in the "fold interference pattern" section.

F_3 Folds

The third generation of folding was the least intense and the most difficult to recognize structurally. Because of the weak nature of the third generation of folding, F_3 fold axes and S_3 crenulation cleavage planes were not directly measurable from outcrop. L_3 lineations, defined by the intersection of S_3 crenulation cleavage planes with S_1 foliation planes, were used to calculate the orientation of the axial surface of the third generation of folding (Figure 17C). As deduced from fold interference patterns and L_3 lineations, F_3 folds are cylindrical and open (interlimb angle equals 70° to 120°), with subhorizontal to moderately plunging fold axes and a nearly upright axial surface that strikes northwest-southeast (average strike = 323°). L_3 lineations plunge in two directions, 180° from each other, because they are the manifestation of an upright axial surface intersecting the S_1 foliation planes on the limbs of F_2 folds.

Brittle deformation features are observed in the study area, mainly in underground exposures. The brittle features include major

fault zones (e.g. the Bear Gulch Fault and the East Fault Zone), minor shear zones, and jointing. These brittle features have been interpreted to be the result of near-surface deformations that formed during the uplift of the Beartooth Block (Laramide Orogeny).

Summary

The Archean metasedimentary rocks in the study area have experienced three Precambrian compressional deformations evidenced by minor fold structures and one later semi-brittle deformation that formed kink bands. Minor structures (F_1, F_2, S_1, S_2, L_2, L_3, L_n-mineral lineation) were observed and measured in surface and underground outcrops in order to define the styles and orientations of the three generations of folding as well as interference patterns (discussed below), which were created during the three compressional deformations. Brittle deformational features in the form of major fault zones, minor shear zones, and joints, formed in conjunction with the Laramide uplift of the Beartooth Block.

STRUCTURAL INTERPRETATION

Fold Interference Pattern

The term superposed folding implies a structural history in which an earlier set of folds is refolded by a later deformational event resulting in complex fold structures, or two directions of folding occur simultaneously, resulting in a complexly folded surface. Complex fold structures are common in orogenic zones where rocks typically experience multiple episodes of deformation. The deformational events may take place as a series of individual deformations separated by large intervals of time, for example, when an earlier orogenic zone is deformed by a later orogeny. Superposed folding may also be the result of progressive deformation in one orogenic cycle. In this scenario, deformation occurs in a series of pulses of finite shortening while, simultaneously, the principal stress directions change with respect to earlier-formed folds. The Late Archean collisional orogeny, postulated for the western margin of the Beartooth Block by Mogk et al. (1988), supports the latter scenario for the deformation of the Jardine rocks.

The geometric fold form observed in hinge-perpendicular section, found in the more micaceous lithologies in the Jardine region, is most closely related to Class 2, similar folds (Ramsay, 1962b, 1967). This fold type is common in zones of regional tectonism and metamorphism where rocks have undergone ductile deformation in a high pressure and temperature environment (Ramsay, 1967). Again, this conforms to the model of Mogk et al. (1988), which involves

deep-seated, orogenic-related deformation of the metasedimentary rocks along the southwestern margin of the Beartooth Block.

The geometry of complex structures produced by the superposition of two successive fold generations is a three-dimensional fold interference pattern that can be recognized in outcrop (Ramsay, 1958; Tobisch, 1966). Four end-member types of fold interference patterns have been defined (Ramsay, 1962a, 1967; Ramsay and Huber, 1987). The final geometric form of the interference pattern depends primarily on the relative orientations of two structural features: first, the angle between the axial plane of the earlier fold and the direction of displacement of the second phase of folding (direction of displacement is referred to as a_2 in Figure 18); and second, the angle between the earliest fold hinge line (F_n) and the later fold hinge line (F_{n+1}) direction (F_{n+1} is referred to as b_2 in Figure 18) of the later fold (Ramsay, 1962a, 1967; Ramsay and Huber, 1987).

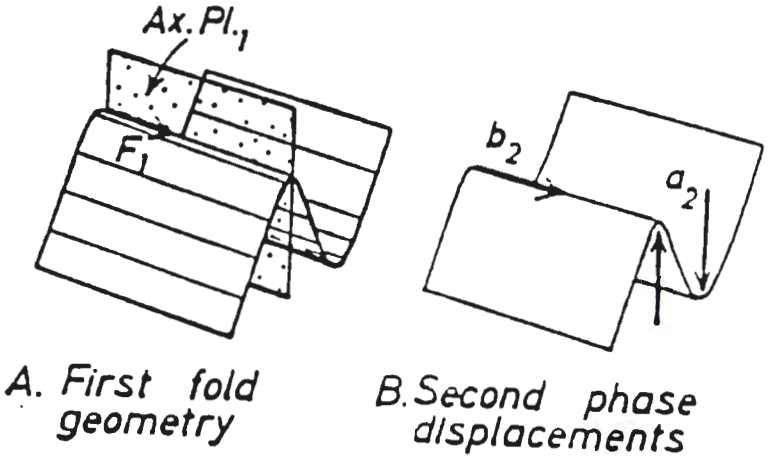

Figure 18. A diagrammatic representation of an initial fold geometry and a second phase of folding, with their respective geometric elements labeled (From Ramsay and Huber, 1987).

In the study area, outcrops displaying a fold interference pattern developed by the superposition of the three fold events are rare. One small outcrop on Germania (location of Germania shown on Figure 2) exhibits a model fold interference pattern that demonstrates clearly the geometrical relationships of Precambrian deformational events experienced by the metasedimentary rocks of the Jardine region.

The outcrop on Germania shows a Ramsay type 1 dome and basin fold interference pattern developed on nearly continuous S_1 foliation planes. This outcrop is illustrated well with pictures taken in two directions, one parallel to the trend of L_2 intersection lineations (Figure 19A), and the other parallel to the trend of L_3 intersection lineations (Figure 19B). The dome and basin fold interference pattern is also illustrated by a three-dimensional contour map of the S_1 foliation, generated from elevation measurements of the S_1 foliation plane below a horizontal reference plane (Figure 20). Minor fold structures show that the domes and basins are formed on the S_1 foliation plane by the superposition of F_3 folds upon, and at a high angle to, F_2 folds.

On the S_1 foliation plane, one can see northeast-southwest trending L_2 intersection lineations running the full length of the outcrop (Figure 19A). The L_2 intersection lineations maintain a straight trace over the topography of the undulatory outcrop, thus showing that F_2 axial surfaces (S_2) is very steep, nearly vertical. The same holds true for the L_3 intersection lineations. Northwest-southeast trending L_3 intersection lineations maintain a straight

A

B

Figure 19. Dome and basin outcrop on Germania. A) Photograph taken parallel to the trend of L_2. B) Photograph taken parallel to the trend of L_3.

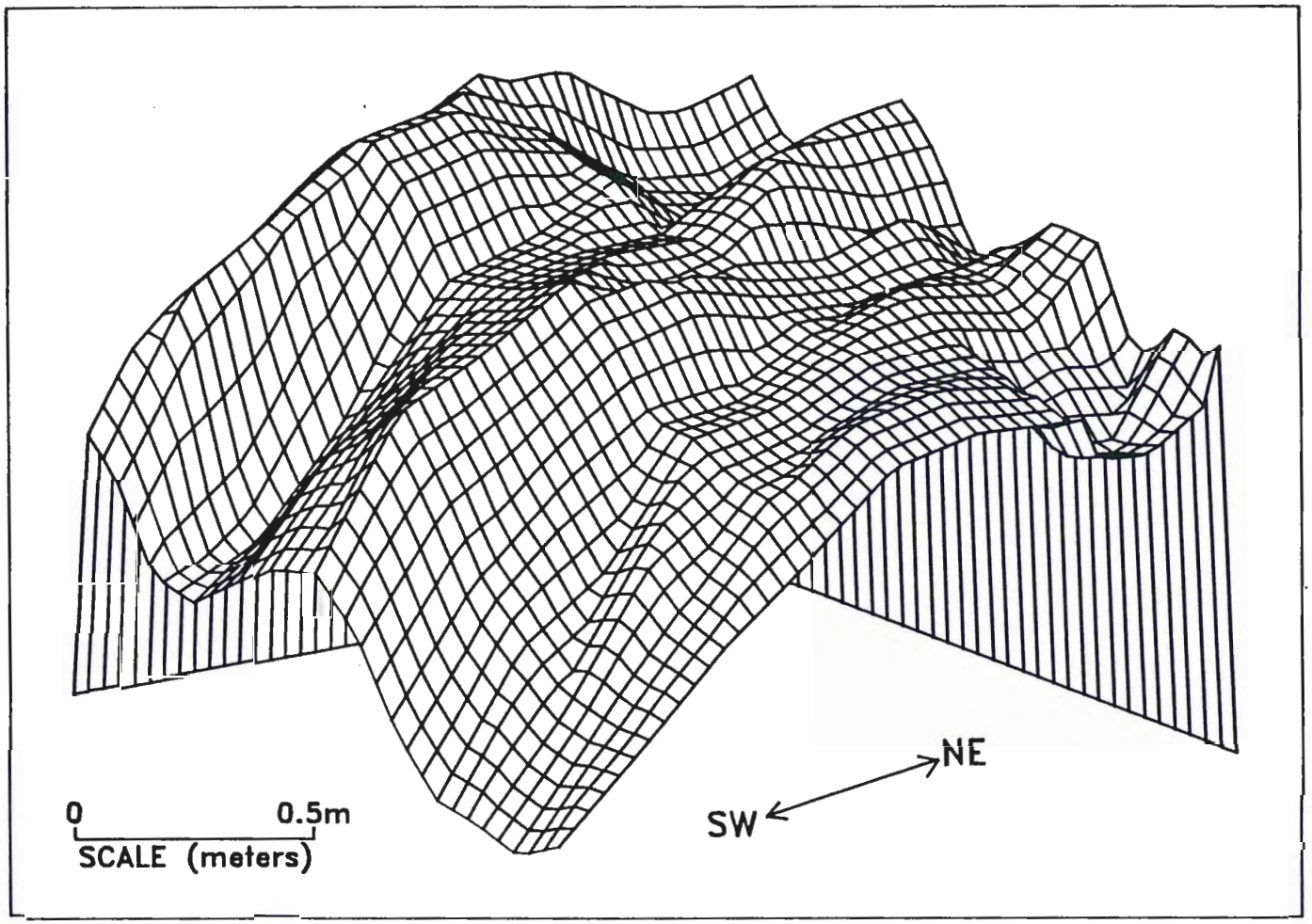

Figure 20. Three dimensional illustration of the dome and basin outcrop on Germania.

trace over the topography of the domes and basins (Figure 19B), demonstrating F_3 axial surfaces (S_3), like the F_2 axial surfaces, is nearly vertically.

Figure 21A is a picture looking down on the same outcrop, showing the near perpendicular relationship between L_2 and L_3 intersection lineations. Figure 21B shows a stereoplot of L_2 and L_3 intersection lineations measured from the dome and basin outcrop. A bestfit great circle through plotted L_2 and L_3 intersection lineations shows that both S_2 and S_3 are nearly vertical (both dipping at approximately 85°) and are also nearly orthogonal to each other.

The shape of the domes and basins is dependent on the shapes and orientations of the two superimposed fold sets. To generate perfectly round domes and basins, one would have to superimpose two fold phases with mutually perpendicular axial surfaces and equal fold amplitudes and wavelengths (Tobisch, 1966). This is very unlikely to occur in nature. As an example, the dome in the middle of the outcrop on Germania (see Figures 19A and 19B) is more elongate than round. This is due to the unequal fold intensities, amplitudes, and wavelengths of the two (F_2 and F_3) superimposed fold phases.

It is important to note that the dome and basin fold interference pattern in this outcrop is being defined by the S_1 foliation plane, not the S_0 bedding plane. The fold interference pattern defined by the S_0 bedding plane is a more complex pattern that involves more than just domes and basins. A fold history of the S_0 bedding surface is

A

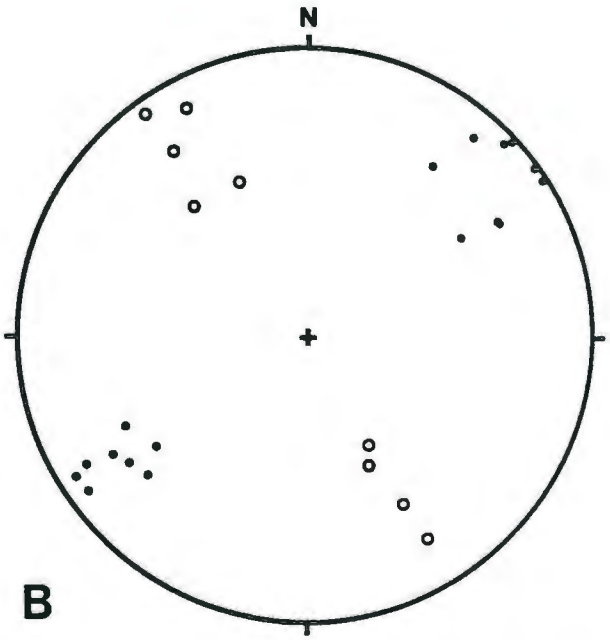

B

Figure 21. A) Photograph looking down at dome and basin outcrop on Germania, showing L_2 (parallel to bottom of photo) and L_3 (parallel to sides of photo) intersection lineations on S_1. B) Stereoplot of L_2 (filled circles) and L_3 (open circles) intersection lineations on S_1 at the dome and basin outcrop on Germania.

discussed in detail in the "Precambrian structural history of the Jardine region" section below.

F_1 folds observed in underground exposure reach a few meters in amplitude and/or wavelength, those inferred from drill core (e.g. Figure 16) reach scales of several hundred meters. Both the observed and inferred folds are obviously isoclinal in nature. The ubiquitous nature and prominence of the S_1 schistosity in the region, a schistosity demonstrably axial-planar to meso-scale F_1 folds, suggests that larger, perhaps kilometer-scale F_1 folds are present. Indeed, the paucity of F_1 fold hinges in the region suggests that F_1 fold limbs are quite large.

F_1 fold axial surfaces, where observed or inferred, are not now always in a horizontal, or subhorizontal orientation. If later F_2 and F_3 folding is removed, however, F_1 fold axial surfaces are subhorizontal. This is the case for the dome and basin outcrop illustrated in Figures 19 and 20. In addition, the likelihood of the existence of large-scale F_1 folds suggests that their axial surfaces were initially of low dip, as upright, isoclinal folds of amplitude greater than a few tens of meters are rare. Thus, the F_1 fold phase likely involved development of isoclinal, recumbent folds, from scales of meters to perhaps kilometers.

Age Relationships Between Fold Events

An age relationship between superimposed fold generations is most often determined by observing the deformation of earlier structural or mineralogical features (e.g. buckling of fold axes and/or

fold axial surfaces, bent or kinked micas) by later periods of deformation (Ramsay, 1958; Tobisch, 1966). One must be cautious when unravelling the structural history of a deformed terrane; what may seem to be undisputed evidence for two periods of deformation may in fact be the result of a single progressive deformational event (Ramsay, 1967; Williams, 1985; Ramsay and Huber, 1987; Marshak and Mitra, 1988).

Microstructural relationships observed in thin section were used in an attempt to resolve the age relationship problem. The objective was to find metamorphic minerals (porphyroblasts) unique to individual generations of folding. If characteristic porphyroblasts were found, their relationship with the fabric in the rock (i.e. pre- syn- or post-kinematic mineral growth) should have given evidence for an age relationship between fold phases. This approach was not applicable to the rocks in the Jardine region because mineral growth occurred only during, and perhaps shortly after, the first generation of folding. Thin section observations failed to show new metamorphic mineral growth occurring during the last two generations of folding.

The structures observed in the metasedimentary rocks of the Jardine region can be resolved into three separate deformational events, each evidenced by a fold generation and its associated minor structures. Minor structures (i.e. pervasive schistosity, crenulation cleavages, minor fold axes, intersection lineations) that formed during each deformation were used in an attempt to define the

relative temporal relationship between the three recognized fold events.

It can be demonstrated that the phase of folding herein labeled F_1 is in fact the first generation of folding in the Jardine region. It is obvious in microscopic and mesoscopic samples that structures formed during the F_1 fold event (the S_1 foliation plane and F_1 fold axes) have been deformed by the two subsequent fold generations. Early fold events (F_1) involving isoclinal and recumbent folding are common in deformed Precambrian terranes (e.g. Hobbs et al., 1976; Hudleston et al., 1988; Holst, 1984; Bauer, 1985).

Determining an age relationship between the last two fold events poses the most difficulty. The difficulty arises because the axial surfaces of each of the last two fold events are perpendicular to each other and the direction of displacement for each fold event lies close to, or within, the axial surface of the other fold.

Imagine a piece of paper being folded twice. The first folds have horizontal axes and upright axial surfaces that trend north-south, while the second folds, whose axes and axial surfaces are also horizontal and upright, trend east-west. The resultant fold interference pattern developed by the superposition of these folds is a Ramsay type 1, dome and basin pattern. If a new piece of paper is folded, but this time the east-west-trending folds are the first folds to develop and the north-south-trending folds develop later, the result is the same dome and basin fold interference pattern. The final orientation of fold axes from each generation of folding is also the same in either case. When two superimposed folds produce a

dome and basin fold interference pattern, minor structures of the earlier fold are not necessarily deformed in such a way as to demonstrate that they were formed previous to the later fold deformation. When overprinted minor structures are analyzed (i.e. fold axes and intersection lineations), the minor fold interference pattern (dome and basin) that they create is reproducible by allowing either fold generation to be first and the other second.

A method that is sometimes used for determining the relative age relationship between fold generations is through the down-plunge observation of minor fold asymmetries (S- and Z-folds) and the superposition of minor folds of the two fold phases (Marshak and Mitra, 1988). By observing asymmetric minor fold interference patterns in outcrop (Z on Z, Z on S, S on S, or S on Z folds), one should be able to discriminate which fold generation was responsible for a particular fold asymmetry and also tell, by fold interference relationships, a relative age relationship between fold generations. This method failed to resolve the age relationship problem between F_2 and F_3 in the Jardine region, because none of the outcrops in the study area displayed asymmetric minor folds, let alone asymmetric minor fold interference patterns.

In multiply deformed terranes, one usually expects to see an axial planar structure (i.e. mineral foliation or cleavage) of the earlier set of folds deformed by later generations of folding. The S_2 axial planar crenulation cleavage in the Jardine region is not noticeably deformed by the third generation of folding because of the orientation of S_2 relative to the displacement direction of the F_3 folds.

Ramsay (1960, 1967) shows that the fold amplitude in a marker plane is dependent on the relative orientation between the marker plane and the displacement direction of the fold phase. If the displacement direction is normal to the marker plane, fold amplitude will be a maximum. If the displacement direction lies within the marker plane, the planar surface will not be folded and only internal deformation of the marker plane will occur (Ramsay, 1960, 1967). The latter is the case for the dome and basin fold interference pattern seen on the S_1 foliation plane in the Jardine region. The displacement direction of F_3 folds lies nearly within the axial planar surface defined by S_2 crenulation cleavages. Likewise, the displacement direction of the F_2 folds lies nearly within the axial planar surface defined by S_3 crenulation cleavages. Neither S_2 nor S_3 crenulation cleavages show any evidence of having been deformed by a later phase of folding.

The labeling scheme used in this report for the last two phases of folding has been based on outcrop observations of minor fold structures and geologic intuition. First, with the labeling scheme used in this report, it can be seen that fold intensity decreased with time. The first phase of folding was the most intense, with isoclinal and recumbent folds developed, the second phase of folding was moderately intense, with close and upright folds developed, and the third phase of folding was the least intense, with open and upright folds developed. This relationship in a multiply-deformed terrane has been noted by Weiss (1959), Hobbs et al. (1976), and Marshak and Mitra (1988). From Hobbs et al., p. 407, 1976:

"First-generation folds are commonly tight to isoclinal and may have slaty cleavage or a schistosity as axial plane foliation. These folds are usually followed, at any given place, by one or more generations of folds having a crenulation cleavage as axial plane foliation. Such folds are commonly more open than the first-generation folds, but they may also become very tight, . . . Finally, there may be one or more generations of folds that lack an axial plane foliation. . . . the late folds may be open warps with rounded hinges and curved limbs. . . . Large first-generation folds are often said to be tight to isoclinal, particularly in medium-grade terrains. There is usually maximum uncertainty about the shape of these folds, or even of their existence, however. Large folds of the second group have more open profiles and more steeply dipping axial surfaces. Late folds of large size tend to be very open and to have steeply dipping axial surfaces."

Also, if the weak F_3 phase of folding and its associated S_3 axial planar crenulation cleavage were folded by the more intense F_2 phase of folding, would not one expect to see the S_3 axial surfaces at least buckled? As mentioned above, there is no observable deformation of S_3.

Precambrian Structural History of the Jardine Region

The S_1 foliation plane is the one feature that provides the most information about the structural history of the Jardine region. The S_1 schistosity, which is found in all rock types, was formed during the first phase of folding and was subsequently deformed by later folding events as well as late stage kinking. It is also the surface on which the fold interference pattern for the region is best observed in outcrop.

Figure 22 diagrammatically illustrates the history of origin and deformation of the S_1 foliation plane in the Jardine region through the three fold phases. The first phase of folding (F_1) involves isoclinal recumbent folds. Since the S_1 foliation plane was formed in an axial-planar geometry to an isoclinal phase of folding, it is also subparallel to bedding (S_0) in all but the hinge zone (Figure 22). The paucity of F_1 hinges indicates that the amplitude of F_1 folds was fairly large (relatively long distance between fold hinges) resulting in a geometry where most of the region is on the limb of an F_1 fold. The inferred amplitude of the F_1 fold as well as the F_2/F_3 fold interference pattern developed on S_1 surfaces supports the idea that F_1 folds were recumbent. Obviously, the S_1 foliation plane contains no F_1 fold hinges, has experienced only two later fold deformations, and therefore has a simpler fold history than the bedding plane (S_0).

The second phase of folding was close and upright, with a nearly horizontal fold axis (Figure 22). This phase of folding created nearly cylindrical northeast-southwest trending folds in the S_1 surface. The axial plane (S_2) of the second phase of folding (F_2) is defined by a zonal crenulation cleavage of the S_1 schistosity. Evidence for mineral recrystallization during the second phase of folding was not found.

The third phase of folding (F_3) was open and upright, with a nearly horizontal fold axis (Figure 22). The S_3 axial surface, which trends northwest-southeast, is defined by a zonal crenulation cleavage of S_1 schistosity. F_3 fold axes are nearly perpendicular to F_2 fold axes and S_3 is nearly perpendicular to S_2. Evidence for

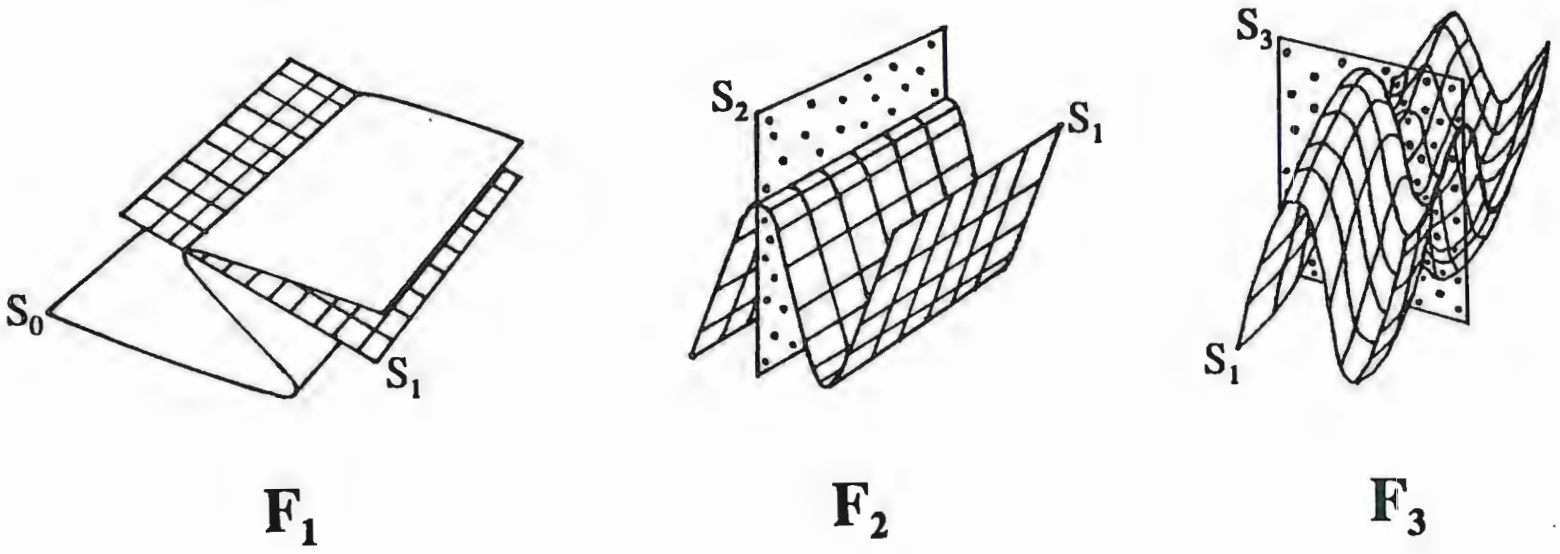

Figure 22. Illustrated history of origin and deformation of S_1 foliation plane.

metamorphic mineral growth during the third phase of folding was not found.

The superposition of F_2 and F_3 phases of folding upon the S_1 foliation plane, created a dome and basin fold interference pattern (Ramsay type 1) defined by the S_1 schistosity (Figures 19A, 19B, and 22). The trend of subhorizontal F_1 fold axes relative to the fold axes of later phases of folding has no influence on the final fold interference pattern seen in S_1. The superposition of the second and third fold phases resulted in fold axes of each of these generations plunging gently to moderately in opposite directions (Figures 22 and 23) whereas the fold axes of either phase would be subhorizontal in the absence of the other fold phase.

The fold history as defined by bedding (S_0) is very similar to the fold history that is defined by the S_1 schistosity, because S_1 is subparallel to S_0 (Figure 23). The fold history of the bedding (S_0) is slightly more complex than the fold history of the S_1 schistosity because the bedding plane (S_0) has undergone three phases of folding while the S_1 schistosity has been affected by only the later two phases of folding. For the most part, S_0 displays a dome and basin fold interference pattern over a majority of its area, it is only in the vicinity of an F_1 fold hinge that the fold interference pattern becomes more complex. Near the F_1 fold hinge, S_0 displays a combination of Ramsay type 2 and type 3 fold interference patterns (Figure 23) (Ramsay, 1962a, 1967; Ramsay and Huber, 1987). The order of fold interference types (Ramsay type 2 and type 3) imposed

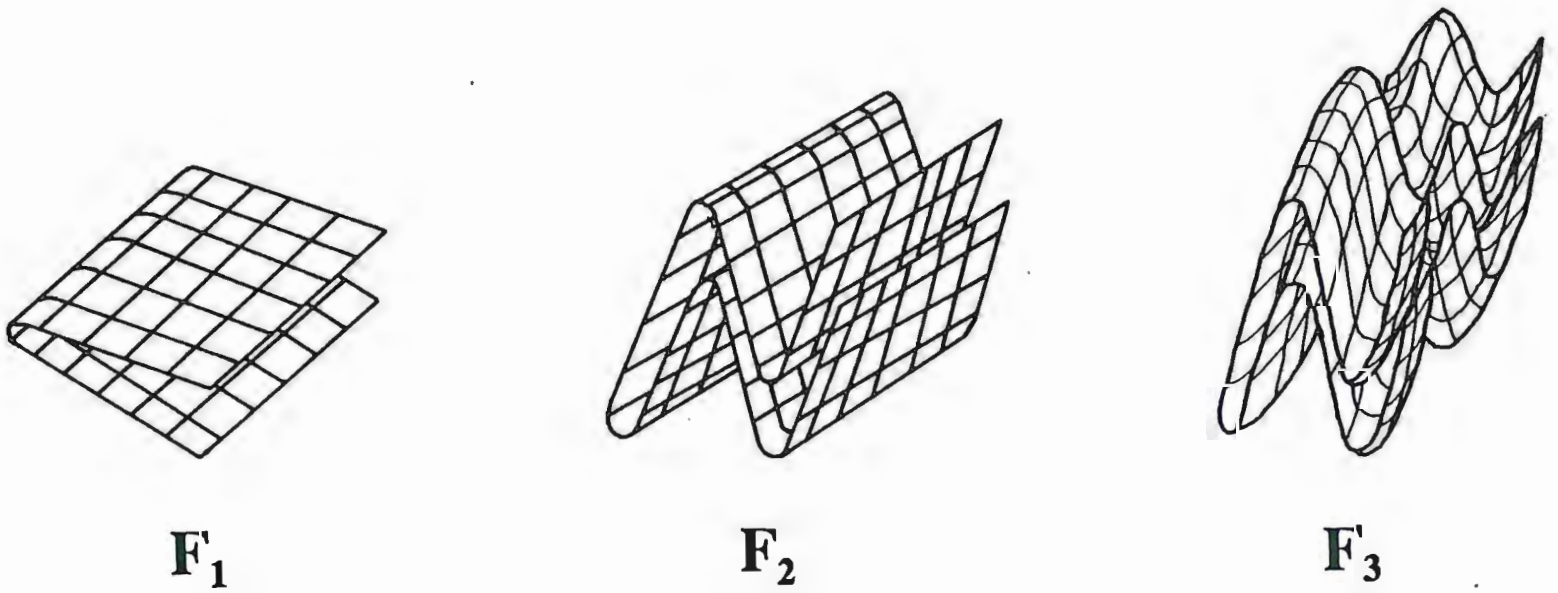

Figure 23. Illustrated history of the deformation of S_0 bedding plane.

upon S_0 after F_1 folding is dependant on the orientation of the F_1 fold axis relative to the fold axis of the second phase of folding. If the F_1 fold axis was colinear with the second phase of folding, a type 3 fold interference pattern would have formed first, followed by a type 2 fold interference pattern in response to the third phase of folding. If the F_1 fold axis was at a high angle to the second phase of folding, a type 2 fold interference pattern would have formed first, followed by a type 3 fold interference pattern in response to the third phase of folding. Because the attitude of the F_1 fold axis, previous to F_2 and F_3, is unknown, the order of fold interference patterns described above is also unknown. It is likely that both scenarios would pertain because as was described earlier, underground observations show that F_1 folds are not cylindrical, but were quite likely sheath folds. The important point is that independent of the orientation of the fold axes of the second and third fold phases relative to F_1 fold axes, the resultant final fold interference pattern displayed by S_0 is predominantly a type 1 dome and basin pattern with minor areas of type 2 and type 3 patterns proximal to the F_1 fold hinges (Figure 23).

Following the three Precambrian phases of folding, a final semi-brittle deformational event formed kink bands. The occurrence of kink bands in surface outcrop is rare, and no kink bands have been reported from underground exposures. The scarcity of observable kink bands makes a structural interpretation of this feature and its associated deformational event, impossible.

The last major deformational event to occur in the Jardine region was the Laramide Orogeny. Uplift of the Beartooth Block during the

Laramide Orogeny caused the formation of near-surface brittle deformation structures. Underground exposures in the Mineral Hill Mine display best the occurrence of major fault zones and minor shear zones. For example, the Bear Gulch Fault on the west side of Mineral Hill is manifest as a 10 m wide fault breccia and gouge zone. Major fault zones were not seen in surface outcrop, while minor shear zones could occasionally be observed. Major fault zones have been inferred in topographic features such as stream valleys (Mineral Hill Mine's Structural Photogeological Interpretation map of the Jardine region, by J. A. E. Allum, 1985), but their existence in these places is still speculative.

CONCLUSIONS

The Archean metasedimentary rocks of the Jardine region have experienced a minimum of three Precambrian ductile deformational events, resulting in three recognizable phases of folding. Evidence for the three phases of folding is in the form of planar and linear structural elements observed in surface and underground outcrops.

The first phase of folding was isoclinal and recumbent. A region-wide, pervasive, axial planar schistosity (S_1), which formed during the F_1 fold event, is subparallel to bedding (S_0). F_1 fold hinges were not observed in surface outcrops, but minor F_1 fold hinges could be seen in underground exposures.

The presence of a region-wide, nearly bedding-parallel schistosity, and the lack of major F_1 fold hinges in outcrop, suggest that F_1 folds are of a large, perhaps kilometer scale. The large-scale and recumbent attitude of F_1 folds allows the term "fold nappe" (Hobbs et al., 1976; Dennis et al., 1981) to be used when defining the first phase of folding in the Jardine region (Holst, 1984). Since the metasedimentary rocks of the southwestern Beartooth Block are an allochthonous package that was initially deformed at a depth of approximately 11 km (depth was calculated using a pressure of 2.9 kb (from above) in the equation P(MPa) = 0.02646 × depth(meters), where P = pressure and 1 kb = 100 MPa; Peacock, 1989), it is neither surprising nor unexpected, that regional-scale nappe development occurred during the first phase of deformation.

Both the second (F_2) and third (F_3) phases of folding were nearly upright with gently plunging fold axes. S_2 and S_3 are nearly orthogonal to each other and their intersection is approximately normal to the inferred undeformed geometry of the axial surface (S_1) of F_1.

Kink bands were observed at two locations in the study area. Their crosscutting relationship with earlier structural features indicates that they are part of a post-F_3 deformational event.

The superposition of the three phases of folding resulted in a Ramsay type 1 dome and basin fold interference pattern that is defined by S_1 and most of S_0 (Figures 22 and 23). S_0 also displays a combination of type 2 and type 3 fold interference patterns near the F_1 fold hinges (Figure 23). Evidence of type 2 and type 3 interference patterns can be seen in cross sections through Mineral Hill as defined by the folded iron formation horizon.

A relative age relationship between the last two phases of folding (F_2 and F_3) could not be unequivocally determined in this investigation. The lack of metamorphic mineral growth during either one or both of the fold phases and the perpendicular orientation of planar and linear structural elements relative to each other, made an age determination unattainable. Thus, the labeling scheme used in this report is based on the author's intuition, along with reports by other investigators (Weiss, 1959; Hobbs et al., 1976; Marshak and Mitra, 1988) who have described situations in which fold intensity decreased with each successive phase of folding.

The pressure and temperature of metamorphism was calculated using data from microprobe analyses from two samples collected on Bald Mountain. The pressure and temperature of peak metamorphism in the study area was approximately 2.9 kb and 560°C. A pressure of 2.9 kb can be interpreted as a maximum depth of burial of approximately 11 km. Caution must be exercised in the interpretation of these numbers, however, since they are dependant on the location of the andalusite-sillimanite reaction. Microstructural observations of fabric/porphyroblast relationships show that the peak of metamorphism occurred during or shortly after the first phase of folding.

The Mineral Hill Mine is in a small structural domain that is bounded to the west by the Bear Gulch Fault and to the east by the East Fault Zone. Both of these steeply dipping dip-slip faults are believed to be associated with the Laramide orogeny. The displacement across either of these two faults has eluded previous investigators because an undeformed and unambiguous marker horizon, with which to measure displacement, does not exist in the area. A correlation across either fault zone, using the iron-formation as a marker horizon, has been attempted and has proven ineffective for reasons described above.

A possible marker horizon for measuring fault displacement may be through the use of a metamorphic isograd. The staurolite isograd was crossed in Mineral Hill (diamond drill hole J-71) at a down-hole depth of 2032 feet (equal to an elevation of approximately 5550 feet above MSL). It has been shown that a staurolite isograd exists

somewhere on or above Bald Mountain. If the staurolite isograd on Bald Mountain is at or above Bald Mountain's peak (the elevation at the top of Bald Mountain equals 8550 feet above MSL), a minimum displacement of approximately 3000 feet may have occurred along the East Fault Zone.

Figure 24 represents an idealized pressure-temperature-time (P-T-t) path for the metamorphic history of the metasedimentary rocks in the Jardine region. Following the deposition of the greywacke sequences and iron formation at the surface, rapid burial was initiated by crustal shortening during a collisional orogenic event. During the burial phase, the rocks experienced a rapid increase in pressure with little or no increase in the temperature. Following the burial phase, the thickened crust was isobarically heated (e.g. 20 Myr. in the Eastern Alps; England and Thompson, 1984) before the onset of erosion and subsequent uplift of the buried rocks occurred. The andalusite-sillimanite facies metamorphism that these rocks experienced during deep-seated metamorphism and deformation, suggests that the initial geothermal gradient was higher than normal, heat was being transferred through the rocks by the circulation of fluids (either magmatic fluids or hydrothermal aqueous solutions), and that rapid uplift of the buried material, possibly by large amplitude folding, occurred (England and Thompson, 1984; Thompson and England, 1984). The circulating hydrothermal fluids mentioned above may be associated with partial-melting of the lower crust during homogeneous thickening (England and Thompson, 1984; Thompson and England, 1984). This could possibly be the

source of the auriferous fluids that circulated through and deposited gold into the iron formation.

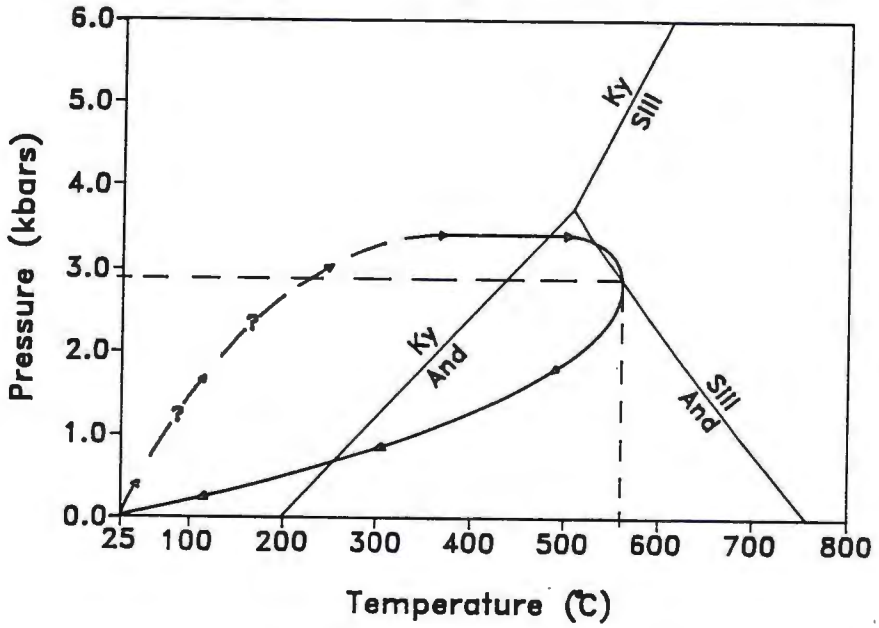

Figure 24. Idealized P–T–t path for the metasedimentary rocks in the Jardine region.

The Archean metasedimentary rocks of the Jardine region exhibit a metamorphic grade, whole-rock chemistry, and structural style that is anomalous with respect to the rest of the surrounding Beartooth Mountain Range. The metamorphic grade in the Jardine region is upper-greenschist to lower-amphibolite grade, while the rest of the Beartooth Range displays upper-amphibolite to granulite-grade metamorphism. The granulite-grade metamorphism of platform-type sediments in the Quad Creek and Hellroaring Plateau areas (east of Jardine) occurred during the first (3400-3200 Ma) of two orogenic cycles experienced by the Beartooth Mountains (Mogk and Henry, 1988).

Thurston (1986) reports that the whole-rock chemistry of the metasedimentary rocks in the Jardine region shows a higher than normal concentration of Cr, Ni, FeO, and MgO, and a lower than normal abundance of alkalis, relative to metasedimentary rocks in the North Snowy Block. He suggests that the sediments were derived from a mafic to ultramafic source area, possibly an Archean greenstone belt. This interpretation is interesting, as Thurston notes, because the northern Wyoming province does not include an Archean greenstone belt.

The structural history of the metasedimentary package involves an early phase of relatively deep-seated (approximately 2.9 kb, or 11 km) nappe-like folding (F_1), followed by a minimum of two later ductile deformations. Fold nappes and multiply deformed terranes are common in compressional orogenic environments and have been reported in terranes dating from the Precambrian to the Tertiary.

The coincidence of an anomalously low grade of metamorphism, a whole-rock chemistry that indicates a sediment source area from a terrane other than the Beartooth Mountains, and a structural style that implies deep-seated compressional tectonics, together, suggest that the metasedimentary suite of rocks in the Jardine region are allochthonous and that they constitute a terrane that was tectonically juxtaposed against the western margin of an Archean continent (the proto-Beartooth Block, 3400-3200 Ma) during a Late Archean plate collisional orogenic event. The age of this collisional orogenic event is constrained by the emplacement of the crosscutting, undeformed, 2600-2700 Ma old Crevice Mountain Stock. Mogk (1988), Mogk and

Henry (1988), and Mogk et al. (1988) suggest that the collisional orogeny included subduction of oceanic crust with contemporaneous subduction-related magmatism resulting in the emplacement of igneous intrusions (2750-2800 Ma) in the central and eastern regions of the Beartooth Mountains.

REFERENCES CITED

Bauer, R. L., 1985, Correlation of early recumbent and younger upright folding across the boundary between an Archean gneiss belt and greenstone terrane, northeastern Minnesota: Geology, v. 13, p. 657-660.

Berman, R. G., Brown, T. H., and Greenwood, H. J., 1985, An internally consistent thermodynamic data base for minerals in the system Na_2O-K_2O-CaO-MgO-FeO-Fe_2O_3-Al_2O_3-SiO_2-TiO_2-H_2O-CO_2: Atomic Energy of Canada Ltd., Technical Report 377, 62 p.

Berman, R. G., Brown, T. H., and Perkins, E. H., 1987, GE0-CALC: software for calculation and display of pressure-temperature-composition phase diagrams: University of British Columbia.

Brookins, D. G., 1968, Rb-Sr and K-Ar age determinations from the Precambrian rocks of the Jardine-Crevice Mountain area, Southwestern Montana: Earth Science Bulletin, v. 1, p. 5-9.

Casella, C. J., 1969, A review of the Precambrian geology of the eastern Beartooth Mountains, Montana and Wyoming, *in* Larsen, L. H., ed., Igneous and Metamorphic Geology: Geological Society of America Memoir 115, p. 53-71.

Casella, C. J., Levay, J., Eble, E., Hirst, B., Huffman, K., Lahti, V., and Metzger, R., 1982, Precambrian geology of the Southwestern Beartooth Mountains, Yellowstone National Park, Montana and Wyoming: Montana Bureau of Mines and Geology Special Publication 84, p. 1-24.

Cosgrove, J. W., 1976, The formation of crenulation cleavage: Journal of the Geological Society, v. 132, p. 155-178.

Deer, W. A., Howie, R. A., and Zussman, J., 1982, Rock-forming minerals, Second edition, Volume 1A, Orthosilicates: New York, Halstad Press, 919 p.

Dennis, J. G., Price, R. A., Sales, J. K., Hatcher, R., Bally, A. W., Perry, W. J., Laubscher, H. P., Williams, R. E., Elliott, D., Norris, D. K., Hutton, D. W., and Emmett, T., 1981, What is a thrust? What is a Nappe?,

in McClay, K, R., and Price, N. J., eds., Thrust and nappe tectonics: Geological Society of London Special Publication 9, 539 p.

England, P. C., and Thompson, A. B., 1984, Pressure-temperature-time paths of regional metamorphism I. Heat transfer during the evolution of regions of thickened continental crust: Journal of Petrology, v. 25, p. 894-928.

Foose, R. M., Wise, D. U., and Garbarini, G. S., 1961, Structural geology of the Beartooth Mountains, Montana and Wyoming: Geological Society of America Bulletin, v. 72, p. 1143-1172.

Fraser, G. D., Waldrop, H. A., and Hyden, H. J., 1969, Geology of the Gardiner area, Park County, Montana: U. S. Geological Survey Bulletin 1277, 118 p.

Gray, D. R., and Durney, D. W., 1979, Crenulation cleavage differentiation: implications of solution-deposition processes: Journal of Structural Geology, v. 1, p. 73-80.

Hallager, W. S., 1980, Geology of Archean gold-bearing metasediments near Jardine, Montana [PhD dissert.]: Berkeley, California, University of California, 136 p.

Hobbs, B. E., Means, W. D., and Williams, P. F., 1976, An outline of structural geology: New York, John Wiley and Sons, 571 p.

Holst, T. B., 1984, Evidence for nappe development during the early Proterozoic Penokean orogeny, Minnesota: Geology, v. 12, p. 135-138.

Hudleston, P. J., Schultz-Ela, D. D., and Southwick, D. L., 1988, Transpression in an Archean greenstone belt, northern Minnesota: Canadian Journal of Earth Sciences, v. 25, p. 1060-1068.

Marlow, P. C., and Etheridge, M. A., 1977, Development of a layered crenulation cleavage in mica schists of the Kanmantoo Group near Macclesfield, South Australia: Geological Society of America Bulletin, v. 88, p. 873-882.

Marshak, S., and Mitra, G., 1988, Basic Methods of Structural Geology: New Jersey, Prentice-Hall, Inc., 445 p.

Mogk, D. W., 1988, Archean allochthonous units in the Northern and Western Beartooth Mountains, Montana: Montana Bureau of Mines and Geology Special Publication 96, p. 43-51.

Mogk, D. W., and Henry, D. J., 1988, Metamorphic petrology of the northern Archean Wyoming province, southwestern Montana: Evidence for Archean collisional tectonics, *in* Ernst, W. G., ed., Metamorphism and crustal evolution in the western United States: New York, Prentice-Hall, p. 363-382.

Mogk, D. W., Mueller, P. A., and Wooden, J. L., 1988, Archean tectonics of the North Snowy Block, Beartooth Mountains, Montana: Journal of Geology, v.96, p. 125-141.

Montgomery, C. W., and Lytwyn, J. N., 1984, Rb-Sr systematics and ages of principal Precambrian lithologies in the South Snowy Block, Beartooth Mountains: Journal of Geology, v. 92, p. 103-112.

Mueller, P. A., Wooden, J. L., Henry, D. J., and Bowes, D. R., 1985, Archean crustal evolution of the eastern Beartooth Mountains, Montana and Wyoming: Montana Bureau of Mines and Geology Special Publication 92, p. 9-20.

Mueller, P. A., Shuster, R. D., Graves, M. A., Wooden, J. L., and Bowes, D. R., 1988, Age and composition of a Late Archean magmatic complex, Beartooth Mountains, Montana-Wyoming: Montana Bureau of Mines and Geology Special Publication 96, p. 7-22.

Nicholson, R., 1966, Metamorphic differentiation in crenulated schists: Nature, v. 209, p.68-69.

Page, N. J., 1977, Stillwater Complex, Montana: rock succession, metamorphism, and structure of the complex and adjacent rocks: U.S. Geological Survey Professional Paper 999, 79 p.

Page, N. J., and Zientek, M. L., 1985, Petrogenesis of metamorphic rocks beneath the Stillwater Complex: lithologies and structures:

Montana Bureau of Mines and Geology Special Publication 92, p. 55-69.

Peacock, S, M, 1989, Thermal modeling of metamorphic pressure-temperature-time paths: a forward approach, *in* Spear, F. S., and Peacock, S. M., eds., Metamorphic pressure-temperature-time paths: American Geophysical Union, Short Course in Geology, Volume 7, p. 57-102.

Perkins, E. H., Brown, T. H., and Berman, R. G., 1986, PTX-SYSTEM: three programs for calculation of pressure-temperature-composition phase diagrams: Computers and Geosciences, v. 12, p. 749-755.

Ramsay, J. G., 1958, Superimposed folding at Loch Monar, Inverness-shire and Ross-shire: Quarterly Journal of the Geological Society of London, v. 113, p. 271-307.

Ramsay, J. G., 1960, The deformation of early linear structures in areas of repeated folding: Journal of Geology, v. 68, p. 75-93.

Ramsay, J. G., 1962a, Interference patterns produced by the superposition of folds of similar type: Journal of Geology, v. 70, P. 466-481.

Ramsay, J. G., 1962b, The geometry and mechanics of formation of "similar" type folds: Journal of Geology, v. 70, p. 309-327.

Ramsay, J. G., 1967, Folding and Fracturing of Rocks: New York, McGraw-Hill Book Co., 568 p.

Ramsay, J. G., and Huber, M. I., 1987, The techniques of modern structural geology, volume 2, folds and fractures: New York, Academic Press Inc., 700 p.

Reid, R. R., McMannis, W. J., and Palmquist, J. C., 1975, Precambrian geology of North Snowy Block, Beartooth Mountains, Montana: Geological Society of America Special Paper 157, 135 p.

Richmond, G. M., 1986, Stratigraphy and correlation of glacial deposits of the Rocky Mountains, the Colorado Plateau and the

ranges of the Great Basin, *in* Sibrava, V., Bowen, D. Q., and Richmond, G. M., eds., Quaternary glaciations in the United States of America: Quaternary Science Reviews, v. 5, (Quaternary glaciations in the northern hemisphere) p. 99-127.

Seager, G. F., 1944, Gold, arsenic, and tungsten deposits of the Jardine-Crevasse Mountain district, Park County, Montana: Montana Bureau of Mines and Geology Memoir 23, 111 p.

Spear, F. S., and Cheney, J. T., 1989, A petrogenetic grid for pelitic schists in the system SiO_2-Al_2O_3-FeO-MgO-K_2O-H_2O: Contributions to Mineralogy and Petrology, v. 101, p. 149-164.

Spear, F. S., 1989, Petrologic determination of metamorphic pressure-temperature-time paths, *in* Spear, F. S., and Peacock, S. M., eds., Metamorphic pressure-temperature-time paths: American Geophysical Union, Short Course in Geology, Volume 7, p. 1-55.

Thompson, A. B., and England, P. C., 1984, Pressure-temperature-time paths of regional metamorphism II. Their inference and interpretation using mineral assemblages in metamorphic rocks: Journal of Petrology, v. 25, p. 929-955.

Thurston, P. B., 1986, Geochemistry and provenance of Archean metasedimentary rocks in the southwestern Beartooth Mountains [M.S. Thesis]: Bozeman, Montana, Montana State University, 74 p.

Tobisch, O. T., 1966, Large-scale basin-and-dome pattern resulting from the interference of major folds: Geological Society of America Bulletin, v. 77, p. 393-408.

Weiss, L. E., 1959, Geometry of superposed folding: Geological Society of America Bulletin, v. 70, p. 91-106.

Williams, P. F., 1972, Development of metamorphic layering and cleavage in low grade metamorphic rocks at Bermagui, Australia: American Journal of Science, v. 272, p. 1-47.

Williams, P. F., 1985, Multiply deformed terrains—problems of correlation: Journal of Structural Geology, v. 7, p. 269-280.

Wilson, C. W., Jr., 1934, Geology of the thrust fault near Gardiner, Montana: Journal of Geology, v. 42, p. 649-663.

Wooden, J. L., Mueller, P. A., Mogk, D. A., and Bowes, D. R., 1988, A review of the geochemistry and geochronology of Archean rocks of the Beartooth Mountains, Montana and Wyoming: Montana Bureau of Mines and Geology Special Publication 96, p. 23-42.

APPENDIX

Microprobe data from samples BM-2 and BM-3.

*FeO equals FeO + Fe_2O_3.
STDEV equals standard deviation.

SAMPLE BM-2
MINERAL COMPOSITIONS IN WEIGHT PERCENT OXIDES

BM-2 Biotite

															AVERAGE	
SiO2	35.30	32.84	34.57	33.80	34.79	35.31	33.57	34.50	34.81	34.06	36.00	33.45	35.16	33.35	34.39	SiO2
TiO2	1.16	1.69	1.52	1.53	1.39	0.70	0.93	1.20	1.31	1.27	1.33	1.50	1.39	1.34	1.30	TiO2
Al2O3	20.92	18.95	19.10	19.06	20.17	19.60	19.39	19.41	19.62	18.63	20.71	18.18	19.70	18.17	19.40	Al2O3
*FeO	17.35	19.28	19.24	20.11	18.33	18.85	19.59	20.12	19.74	21.69	20.11	20.23	19.98	21.11	19.70	*FeO
MnO	0.11	0.03	0.03	0.13	0.03	0.00	0.00	0.03	0.08	0.09	0.00	0.00	0.00	0.00	0.04	MnO
MgO	8.73	9.08	9.24	9.66	9.87	9.65	9.16	10.11	9.73	9.65	9.34	9.48	9.48	9.45	9.47	MgO
CaO	0.00	0.00	0.00	0.00	0.00	0.00	0.00	0.00	0.00	0.00	0.00	0.00	0.00	0.00	0.00	CaO
Na2O	0.38	0.00	0.21	0.00	0.25	0.31	0.14	0.60	0.34	0.09	0.38	0.31	0.27	0.33	0.26	Na2O
K2O	7.89	8.53	8.48	7.91	8.97	8.41	8.52	8.71	9.22	8.64	8.49	9.22	9.34	8.67	8.64	K2O
Total	91.84	90.40	92.39	92.20	93.80	92.83	91.30	94.68	94.85	94.12	96.36	92.37	95.32	92.42	93.21	Total

BM-2 Garnet

																	AVERAGE	
SiO2	36.34	35.85	36.27	37.16	36.14	35.75	37.17	36.86	37.35	38.09	36.61	37.64	36.32	34.90	36.94	36.98	36.65	SiO2
TiO2	0.00	0.12	0.02	0.00	0.12	0.18	0.00	0.05	0.03	0.03	0.00	0.12	0.10	0.03	0.12	0.12	0.07	TiO2
Al2O3	21.76	21.19	21.32	21.36	20.91	21.62	20.79	20.59	20.45	20.52	20.80	20.07	20.01	20.39	20.47	20.74	20.81	Al2O3
*FeO	34.55	35.66	35.51	34.98	36.83	36.07	34.62	36.16	36.04	37.14	36.39	36.67	35.74	36.84	36.20	36.74	36.01	*FeO
MnO	1.80	1.82	1.67	1.98	1.97	1.86	2.20	1.95	2.05	2.20	2.10	2.05	2.14	1.87	2.00	1.64	1.96	MnO
MgO	2.62	2.32	2.36	2.41	2.37	2.22	2.55	2.24	2.52	1.91	2.15	1.97	2.79	2.66	2.98	2.82	2.43	MgO
CaO	1.05	1.07	1.16	1.07	1.27	1.08	1.13	1.22	1.17	1.26	1.23	1.09	1.43	1.09	1.14	1.26	1.17	CaO
Total	98.12	98.03	98.31	98.96	99.61	98.78	98.46	99.07	99.61	101.15	99.28	99.61	98.53	97.78	99.85	100.30	99.09	Total

BM-2 Staurolite

													AVERAGE	
SiO2	27.87	26.23	26.68	27.54	27.43	28.27	27.07	27.02	26.61	27.01	27.00	25.50	27.02	SiO2
TiO2	0.41	0.46	0.29	0.23	0.58	0.33	0.12	0.42	0.18	0.49	0.53	0.40	0.37	TiO2
Al2O3	53.68	54.02	53.60	53.82	52.51	50.97	50.52	50.94	50.62	51.83	51.50	51.87	52.16	Al2O3
*FeO	15.79	16.39	15.21	15.52	15.10	15.18	14.39	15.25	14.86	15.34	14.59	14.81	15.20	*FeO
MnO	0.14	0.14	0.17	0.13	0.06	0.21	0.14	0.12	0.12	0.27	0.19	0.18	0.16	MnO
MgO	1.29	1.27	1.30	1.45	1.69	1.49	1.77	1.51	1.52	1.50	1.49	1.34	1.47	MgO
CaO	0.09	0.06	0.00	0.03	0.00	0.03	0.00	0.00	0.04	0.00	0.07	0.00	0.03	CaO
ZnO	0.00	0.30	0.00	0.15	0.04	0.21	0.18	0.26	0.23	0.00	0.00	0.28	0.14	ZnO
Total	99.27	98.87	97.25	98.87	97.41	96.69	94.19	95.52	94.18	96.44	95.37	94.38	96.54	Total

SAMPLE BM-3
MINERAL COMPOSITIONS IN WEIGHT PERCENT OXIDES

BM-3	Staurolite																AVERAGE	
SiO2	27.94	26.18	27.54	26.74	26.26	26.17	25.70	24.61	26.56	26.45	27.21	24.75	26.41	25.11	24.14	24.57	26.02	SiO2
TiO2	0.31	0.38	0.50	0.26	0.59	0.71	0.60	0.54	0.64	0.66	0.45	0.58	0.77	0.50	0.65	0.68	0.55	TiO2
Al2O3	54.50	53.89	53.89	53.00	52.23	52.84	54.21	55.23	54.14	53.05	53.66	53.36	54.49	53.71	52.46	54.11	53.67	Al2O3
*FeO	12.92	13.20	13.73	13.07	12.87	12.95	13.64	13.39	13.34	14.06	13.30	13.30	14.21	13.80	13.94	13.60	13.46	*FeO
MnO	0.16	0.41	0.40	0.40	0.55	0.41	0.36	0.28	0.47	0.50	0.45	0.31	0.41	0.38	0.43	0.43	0.40	MnO
MgO	1.40	1.39	1.71	1.50	1.39	1.46	1.48	1.18	1.45	1.55	1.73	1.51	1.33	1.21	1.50	1.41	1.45	MgO
CaO	0.05	0.00	0.02	0.02	0.14	0.00	0.06	0.03	0.05	0.01	0.06	0.01	0.00	0.02	0.00	0.21	0.04	CaO
ZnO	0.51	0.43	0.39	0.51	0.64	0.37	0.40	0.43	0.46	0.48	0.68	0.54	0.50	0.52	0.39	0.58	0.49	ZnO
Total	97.79	95.88	98.18	95.50	94.67	94.91	96.45	95.69	97.11	96.76	97.54	94.36	98.12	95.25	93.51	95.59	96.08	Total

BM-3	Biotite											AVERAGE	
SiO2	33.76	33.87	34.11	33.22	33.43	31.89	30.95	32.73	33.40	32.58	31.98	31.07	32.75	SiO2
TiO2	1.43	1.14	1.20	1.51	1.67	1.66	1.51	1.87	1.60	1.52	1.60	1.63	1.53	TiO2
Al2O3	20.71	24.06	20.50	20.15	21.07	20.53	20.05	20.68	21.45	20.17	20.66	20.09	20.84	Al2O3
*FeO	18.78	17.58	18.64	18.82	19.19	19.51	19.57	17.99	17.44	19.13	19.19	19.87	18.81	*FeO
MnO	0.17	0.09	0.20	0.13	0.18	0.04	0.24	0.13	0.19	0.11	0.00	0.12	0.13	MnO
MgO	9.77	8.67	9.25	9.13	9.66	9.39	9.10	9.63	9.63	8.96	9.63	10.01	9.40	MgO
CaO	0.00	0.00	0.00	0.00	0.00	0.00	0.00	0.00	0.00	0.00	0.00	0.00	0.00	CaO
Na2O	0.11	0.34	0.15	0.08	0.17	0.35	0.35	0.30	0.30	0.19	0.35	0.28	0.25	Na2O
K2O	8.80	8.76	9.00	8.96	8.71	8.63	8.99	9.41	9.20	9.03	7.95	8.80	8.85	K2O
Total	93.53	94.51	93.05	92.00	94.08	92.00	90.76	92.74	93.21	91.69	91.36	91.87	92.57	Total

SAMPLE BM-2
NUMBERS OF IONS ON THE BASIS OF 24 OXYGENS

GARNET

Ti	Mn	Fe	Si	Ca	Mg	Al
0.000	0.250	4.729	5.951	0.183	0.634	4.201
0.014	0.251	4.922	5.915	0.184	0.571	4.123
0.000	0.231	4.879	5.959	0.202	0.578	4.127
0.000	0.271	4.748	6.034	0.186	0.581	4.089
0.014	0.269	5.031	5.904	0.220	0.575	4.024
0.019	0.255	4.954	5.870	0.188	0.540	4.183
0.000	0.302	4.725	6.067	0.196	0.618	4.001
0.004	0.269	4.942	6.026	0.211	0.542	3.968
0.000	0.281	4.891	6.063	0.200	0.609	3.910
0.000	0.296	4.980	6.110	0.216	0.457	3.879
0.000	0.288	4.973	5.980	0.216	0.522	4.004
0.014	0.281	4.985	6.120	0.186	0.477	3.845
0.009	0.295	4.926	5.990	0.251	0.682	3.885
0.000	0.265	5.158	5.841	0.191	0.658	4.019
0.014	0.271	4.904	5.989	0.195	0.718	3.910
0.014	0.223	4.961	5.970	0.213	0.677	3.947
AVERAGE	0.006	0.269	4.919	5.987	0.202	0.590	4.007
STDEV	0.007	0.023	0.112	0.081	0.018	0.073	0.111

TOTAL 15.981

STAUROLITE

Ti	Mn	Fe	Zn	Si	Ca	Mg	Al
0.042	0.017	1.897	0.000	4.011	0.012	0.274	9.113
0.047	0.017	1.997	0.030	3.822	0.008	0.273	9.274
0.030	0.017	1.865	0.000	3.916	0.000	0.280	9.275
0.025	0.013	1.875	0.013	3.980	0.000	0.310	9.171
0.060	0.004	1.850	0.000	4.018	0.000	0.365	9.072
0.035	0.026	1.873	0.021	4.175	0.000	0.325	8.874
0.013	0.013	1.820	0.018	4.094	0.000	0.395	9.009
0.044	0.013	1.911	0.026	4.052	0.000	0.334	9.011
0.018	0.013	1.884	0.022	4.039	0.004	0.343	9.054
0.052	0.030	1.903	0.000	4.008	0.000	0.331	9.070
0.057	0.021	1.820	0.000	4.034	0.008	0.329	9.073
0.044	0.022	1.879	0.026	3.871	0.000	0.298	9.278
AVERAGE	0.039	0.017	1.881	0.013	4.002	0.003	0.321	9.106
STDEV	0.015	0.007	0.047	0.012	0.096	0.004	0.037	0.124

TOTAL 15.382

BIOTITE

Ti	Mn	Fe	Si	K	Ca	Na	Mg	Al
0.143	0.015	2.442	5.948	1.696	0.000	0.119	2.190	4.153
0.221	0.000	2.822	5.753	1.902	0.000	0.000	2.370	3.912
0.195	0.000	2.742	5.894	1.841	0.000	0.065	2.346	3.837
0.196	0.015	2.881	5.792	1.725	0.000	0.000	2.463	3.846
0.172	0.000	2.564	5.820	1.911	0.000	0.078	2.460	3.979
0.084	0.000	2.659	5.957	1.807	0.000	0.099	2.426	3.896
0.117	0.000	2.839	5.820	1.882	0.000	0.045	2.366	3.958
0.147	0.000	2.818	5.780	1.859	0.000	0.191	2.523	3.832
0.162	0.010	2.757	5.819	1.962	0.000	0.108	2.424	3.866
0.160	0.010	3.085	5.792	1.872	0.000	0.025	2.446	3.734
0.163	0.000	2.740	5.868	1.765	0.000	0.119	2.267	3.974
0.193	0.000	2.929	5.796	2.039	0.000	0.102	2.445	3.711
0.170	0.000	2.775	5.844	1.980	0.000	0.083	2.346	3.858
0.173	0.000	3.058	5.780	1.918	0.000	0.106	2.442	3.709
AVERAGE	0.164	0.004	2.794	5.833	1.860	0.000	0.081	2.394	3.876
STDEV	0.035	0.006	0.172	0.063	0.097	0.000	0.052	0.087	0.119

TOTAL 17.014

SAMPLE BM-3
NUMBERS OF IONS ON THE BASIS OF 24 OXYGENS

BIOTITE

	Ti	Mn	Fe	Si	K	Ca	Na	Mg	Al	
	0.178	0.020	2.647	5.690	1.890	0.000	0.029	2.454	4.112	
	0.140	0.009	2.423	5.582	1.838	0.000	0.106	2.128	4.672	
	0.149	0.024	2.639	5.775	1.943	0.000	0.049	2.331	4.090	
	0.191	0.015	2.704	5.711	1.962	0.000	0.025	2.335	4.082	
	0.207	0.024	2.690	5.613	1.863	0.000	0.054	2.415	4.169	
	0.213	0.005	2.823	5.514	1.904	0.000	0.111	2.421	4.184	
	0.197	0.031	2.890	5.469	2.023	0.000	0.114	2.397	4.177	
	0.235	0.015	2.564	5.584	2.048	0.000	0.095	2.444	4.157	
	0.198	0.024	2.458	5.627	1.973	0.000	0.094	2.418	4.258	
	0.193	0.015	2.771	5.645	1.993	0.000	0.061	2.314	4.119	
	0.208	0.000	2.774	5.528	1.750	0.000	0.116	2.480	4.204	
	0.209	0.015	2.894	5.415	1.953	0.000	0.092	2.597	4.126	
	0.299	0.016	2.952	5.310	2.107	0.000	0.026	2.465	4.251	
	0.235	0.021	2.968	5.240	2.075	0.000	0.000	2.470	4.363	
	0.241	0.005	2.925	5.215	2.084	0.000	0.184	2.484	4.333	
AVERAGE	0.206	0.016	2.741	5.528	1.960	0.000	0.077	2.410	4.220	TOTAL 17.159
STDEV	0.038	0.008	0.173	0.170	0.100	0.000	0.048	0.106	0.150	

STAUROLITE

	Ti	Mn	Fe	Zn	Si	Ca	Mg	Al	
	0.034	0.017	1.560	0.051	4.034	0.004	0.301	9.277	
	0.039	0.047	1.634	0.043	3.877	0.000	0.304	9.411	
	0.051	0.046	1.661	0.038	3.985	0.000	0.370	9.195	
	0.026	0.048	1.622	0.052	3.973	0.000	0.331	9.285	
	0.066	0.070	1.613	0.070	3.945	0.022	0.308	9.247	
	0.079	0.048	1.619	0.039	3.910	0.000	0.325	9.312	
	0.065	0.043	1.682	0.043	3.792	0.008	0.325	9.436	
	0.057	0.035	1.665	0.043	3.661	0.004	0.257	9.690	
	0.068	0.056	1.632	0.047	3.887	0.004	0.313	9.338	
	0.073	0.061	1.732	0.052	3.901	0.000	0.337	9.228	
	0.047	0.051	1.620	0.072	3.963	0.008	0.372	9.212	
	0.062	0.035	1.681	0.058	3.739	0.000	0.337	9.506	
	0.081	0.047	1.729	0.051	3.843	0.000	0.286	9.344	
	0.053	0.044	1.729	0.057	3.763	0.000	0.268	9.493	
	0.072	0.054	1.786	0.040	3.698	0.000	0.342	9.480	
	0.074	0.052	1.699	0.061	3.674	0.030	0.312	9.539	
AVERAGE	0.059	0.047	1.667	0.051	3.853	0.005	0.318	9.375	TOTAL 15.374
STDEV	0.016	0.012	0.058	0.010	0.118	0.009	0.032	0.140	